Synchronized clusters in globally connected networks of second-order oscillators

Gao, Jian; Efstathiou, Konstantinos

Published in:
Chaos

DOI:
10.1063/5.0057125

Publication date:
2021

Chaos

Synchronized clusters in globally connected networks of second-order oscillators: Uncovering the role of inertia

Cite as: Chaos **31**, 093137 (2021); https://doi.org/10.1063/5.0057125
Submitted: 18 May 2021 • Accepted: 01 September 2021 • Published Online: 28 September 2021

Jian Gao and Konstantinos Efstathiou

Synchronized clusters in globally connected networks of second-order oscillators: Uncovering the role of inertia

Cite as: Chaos **31**, 093137 (2021); doi: 10.1063/5.0057125
Submitted: 18 May 2021 · Accepted: 1 September 2021 ·
Published Online: 28 September 2021

Jian Gao[1] and Konstantinos Efstathiou[2,a)]

AFFILIATIONS

[1]Bernoulli Institute for Mathematics, Computer Science, and Artificial Intelligence, University of Groningen, P.O. Box 407, 9700 AK Groningen, The Netherlands
[2]Division of Natural and Applied Sciences and Zu Chongzhi Center for Mathematics and Computational Sciences, Duke Kunshan University, No. 8 Duke Avenue, Kunshan 215316, China

[a)]**Author to whom correspondence should be addressed:** k.efstathiou@dukekunshan.edu.cn

ABSTRACT

We discuss the formation of secondary synchronized clusters, that is, small clusters of synchronized oscillators besides the main cluster, in second-order oscillator networks and the role of inertia in this process. Such secondary synchronized clusters give rise to non-stationary states such as oscillatory and standing wave states. After describing the formation of such clusters through numerical simulations, we use a time-periodic mean field ansatz to obtain a qualitative understanding of the formation of non-stationary states. Finally, the effect of inertia in the formation of secondary synchronized clusters is analyzed through a minimal model. The analysis shows that the effect of the main synchronized cluster on the other oscillators is weakened by inertias, thus leading to secondary synchronized clusters during the transition to synchronization.

The synchronization process in oscillator networks, such as in the Kuramoto model, is typically driven by the formation of a large synchronized cluster that gradually absorbs more oscillators. This process can be disrupted by the formation of smaller synchronized clusters that compete with the main one. Such smaller clusters lead to non-stationary states where the order parameter varies periodically in time in contrast to coherent stationary states where it is constant. In this paper, we consider oscillators with inertia and we study the formation of smaller synchronized clusters. We find that inertia plays a crucial role in the formation of such clusters and the increase of inertia leads to a strengthening of the secondary clusters at the expense of the main cluster. We use numerical experiments, a theoretical analysis of the mean-field equations, and a simplified model to explain different aspects of the formation of secondary synchronized clusters and non-stationary states.

I. INTRODUCTION

Synchronization of coupled dynamical units is a prevalent phenomenon in nature (Acebrón *et al.*, 2005 and Arenas *et al.*, 2008) and many mathematical models have been used in its study. Among them, the Kuramoto model (Kuramoto, 1975; 1984; Kuramoto and Nishikawa, 1987; and Rodrigues *et al.*, 2016) is one of the most popular and successful models for the study of synchronization and other collective phenomena.

Second-order Kuramoto oscillators where frequency adaptations (inertias) are added to the Kuramoto oscillators were first proposed in Ermentrout (1991) to describe the dynamics of three tropical Asian firefly species. Since then, this model has found several applications such as Josephson junction arrays (Levi *et al.*, 1978; Watanabe and Strogatz, 1994; and Trees *et al.*, 2005), goods markets (Ikeda *et al.*, 2012), and dendritic neurons (Sakyte and Ragulskis, 2011). One particular field of study where Kuramoto oscillators

with inertia are very relevant is power grids. There is an enormous amount of literature that explore different aspects of this topic, often combined with the issue of stability and control. We indicatively mention the works (Filatrella *et al.*, 2008; Lozano *et al.*, 2012; Witthaut and Timme, 2012; Rohden *et al.*, 2012; 2014; 2017; Menck *et al.*, 2013; Dörfler *et al.*, 2013; Kim *et al.*, 2015; Hellmann *et al.*, 2016; Grzybowski *et al.*, 2016; Maïzi *et al.*, 2016; Manik *et al.*, 2017; Pinto and Saa, 2016; Witthaut *et al.*, 2016; Gambuzza *et al.*, 2017; and Tumash *et al.*, 2018; 2019).

There are several numerical and analytical methods for analyzing the collective behavior of second-order Kuramoto oscillators. Focusing on stationary states, the self-consistent method is one of the most prominent analytical methods for the study of network dynamics, due to its great success for standard Kuramoto oscillators (i.e., without inertia). The self-consistent method was first applied to analyze the stationary states in the model of Kuramoto oscillators with inertias by Tanaka *et al.* (1997a). The self-consistent method in Tanaka *et al.* (1997a) produces accurate results for stationary states away from the zero value of the order parameter, that is, away from the incoherent state. An improvement of the self-consistent method, which extends the predictive power of the method also near incoherent states, was developed in Gao and Efstathiou (2018). This allows the determination of the critical coupling strength for the bifurcation of coherent stationary states from the incoherent state. The self-consistent method leads to quantitative predictions about phenomena such as hysteresis (Olmi *et al.*, 2014) and different types of transition from incoherence to coherence (Tanaka *et al.*, 1997a; 1997b; Acebrón *et al.*, 2000; and Barre and Métivier, 2016).

Beyond the self-consistent method, other analytical approaches have been proposed for the study of Kuramoto oscillators with inertia. For example, Barre and Métivier (2016) determine the linear stability of the incoherent state using an unstable manifold expansion. The same approach has been used in the study of Kuramoto oscillators with inertia and delayed coupling in Métivier *et al.* (2020). Two different analytical methods that also apply to the case of noisy oscillators have been proposed in Munyaev *et al.* (2020).

Other works consider special arrangements that can lead to a radical simplification of the dynamics. For example, Belykh *et al.* (2015) consider oscillators connected in a star configuration, while Brister *et al.* (2020) consider three clusters of identical oscillators. The case of identical oscillators is also studied in Kruk *et al.* (2020) in the context of the appearance of solitary states. A more general case is considered in Medvedev and Mizuhara (2021) focusing on the synchronization of oscillators on Erdös–Rényi graphs, where the natural frequencies are drawn from a bimodal distribution.

As several other earlier works have demonstrated, Kuramoto oscillators with inertia can demonstrate much more complicated dynamics than only stationary states. Two such examples of non-stationary states are oscillatory states and standing waves (Tanaka *et al.*, 1997b; Olmi *et al.*, 2014; and Olmi and Torcini, 2016). In oscillatory states, the coherence r, that is, the modulus of the complex order parameter in Eq. (3), does not attain a fixed value but oscillates around a mean value. In the case of standing waves, the coherence also oscillates but the distinguishing feature is that its value moves periodically between (almost) zero and a maximum value (see, for example, Fig. 11). Such non-stationary states have been found in systems with unimodal distributions of natural frequencies (Tanaka *et al.*, 1997b) but also with bimodal distributions (Olmi and Torcini, 2016), and in complex networks (Olmi *et al.*, 2014). Olmi *et al.* (2014) observed that oscillatory states are associated with the appearance, besides the main cluster, of additional clusters of frequency synchronized oscillators called drifting clusters in Olmi *et al.* (2014) and secondary synchronized clusters in this work.

Non-oscillatory states also appear in first-order Kuramoto oscillators with non-unimodal natural frequency distributions. For this case, Engelbrecht and Mirollo (2012) showed that the dynamics of a single oscillator in a periodic mean field gives rise to a circle map whose resonance tongues correspond to secondary synchronized clusters, and they proceeded to thoroughly analyze the properties of this circle map. Therefore, they established that a periodic mean field is compatible with the existence of secondary synchronized clusters.

In the context of second-order oscillators, not much is known about the relation between secondary synchronized clusters and non-stationary states. How are secondary synchronized clusters formed? Are they compatible with the periodic behavior of the coherence r in non-stationary states such as oscillatory states and standing waves? What is the role of inertia in the formation of secondary synchronized clusters? Our main focus in this paper is to answer these questions: understand the formation of secondary synchronized clusters, the role of inertia in this process, and the connection between secondary synchronized clusters and non-stationary states.

This paper is organized as follows. In Sec. II, we define the studied model of coupled second-order oscillators and we discuss the phenomenology of secondary synchronized clusters and their relation to oscillatory states through numerical simulations of the dynamics, focusing on the effect of inertia. In Sec. III, we consider the dynamics of a single oscillator in a periodically varying mean field and we show that such mean fields are inextricably related to secondary synchronized clusters along the lines of the approach in Engelbrecht and Mirollo (2012). Through the analysis of the dynamics, we give a qualitative explanation of why oscillatory states appear only in the forward process for sufficiently large inertias. Moreover, we discuss the validity of assuming a time-periodic mean field from the point of view of self-consistency. In Sec. IV, we use a minimal model of three oscillators to qualitatively analyze the role of inertia in the formation process of secondary synchronized clusters. We conclude with a discussion of the results in Sec. V. Additional computations and discussion of secondary synchronized clusters for bimodal natural frequency distributions are given in the Appendix.

II. MODEL AND PHENOMENOLOGY

In this paper, we consider Kuramoto oscillators with inertias. The model consists of a finite number of oscillators indexed by $i = 1, \ldots, N$. The state of each oscillator is characterized by a phase $\theta_i \in \mathbb{R}/2\pi\mathbb{Z}$, that is, $\theta_i \in [0, 2\pi]$ with $0 \equiv 2\pi$, and a corresponding angular velocity $\omega_i = \dot{\theta}_i \in \mathbb{R}$. In terms of these variables, the dynamics is given for each $i = 1, \ldots, N$ by

$$\dot{\theta}_i = \omega_i, \tag{1a}$$

$$m\dot{\omega}_i + D\omega_i = \Omega_i + \frac{K}{N}\sum_{j=1}^{N}\sin(\theta_j - \theta_i), \tag{1b}$$

which can be also written as the second-order equation

$$m\ddot{\theta}_i + D\dot{\theta}_i = \Omega_i + \frac{K}{N}\sum_{j=1}^{N}\sin(\theta_j - \theta_i). \tag{1c}$$

In these equations, m is the inertia, D is the damping coefficient, and K is the coupling strength. The quantities Ω_i can be thought of as torques being applied to the oscillators (rotors). When $K = 0$, then the ith oscillator's angular velocity ω_i as $t \to \infty$ becomes Ω_i/D and for this reason, with some abuse of language, we will call Ω_i the "natural frequency" of the ith oscillator. The values Ω_i are randomly chosen from a distribution $g(\Omega)$. Different values of the parameters m, D, K, and different distributions $g(\Omega)$ can lead to different collective dynamics and synchronization scenarios.

In this section, we present the results of numerical simulations that demonstrate the effect of inertia on the appearance of secondary synchronized clusters. In particular, our aim is to demonstrate that increasing the inertia favors the formation of secondary synchronized clusters rather than give a complete description of the transition to synchronization. For a complete numerical study of the synchronization process in such systems, we refer to Olmi *et al.* (2014) and Olmi and Torcini (2016).

We study systems with $N = 10^4$ oscillators and with different values of inertia m fixing the value of the damping coefficient to $D = 1$. Note here that a time rescaling reveals that the effective parameter is the reduced mass $\mu = m/D^2$. However, we choose to keep the two parameters m and D. The natural frequencies of oscillators are chosen randomly from a unimodal distribution $g(\Omega) = G(\Omega; 0, 1)$, where $G(\Omega; \mu, \sigma)$ is the Gaussian distribution

$$G(\Omega; \mu, \sigma) = \frac{1}{\sqrt{2\pi\sigma^2}}\exp\left(-\frac{(\Omega-\mu)^2}{2\sigma^2}\right). \tag{2}$$

A similar analysis for bimodal distributions is presented in the Appendix.

The collective state of the oscillators is described by the (complex) *order parameter*

$$r\,e^{i\phi} = \frac{1}{N}\sum_{j=1}^{N} e^{i\theta_j}. \tag{3}$$

The modulus r of the order parameter measures the phase coherence, and ϕ represents a collective phase. If all the oscillators move in a single tight cluster, we have $r \approxeq 1$, with $r = 1$ corresponding to complete phase synchrony. On the contrary, if the oscillators move incoherently, scattered around the circle, we have $r \approxeq 0$.

For each inertia value and natural frequency distribution, we consider a forward and a backward process (Tanaka *et al.*, 1997a). In the forward process, the initial state of the oscillators is constructed for $K = 0.01$ by drawing the phases θ_i from the uniform distribution in $[0, 2\pi]$ and the frequencies $\omega_i = \dot{\theta}_i$ from the uniform distribution in $[0, 1]$. Then, the system is evolved using a Runge–Kutta fourth-order method with fixed step-size $\delta t = 0.01$ for time $T = 1500$. The transient part of the evolution from $t = 0$ to $t = 1000$ is discarded and only results obtained from the time interval between $t = 1000$ and $t = 1500$ are reported. The choice of initial phases and frequencies for $K = 0.01$ leads to an incoherent state. After $T = 1500$, the value of K is increased by $\delta K = 0.01$ and this procedure is repeated until $K = 10$ with the initial state for $K + \delta K$ being the final state for K.

In the backward process, the initial state of the oscillators is constructed for $K = 10$ by drawing the phases θ_i from a narrow uniform distribution supported on $[0, 2\pi/100]$ and the frequencies ω_i from the uniform distribution supported on $[0, 1]$. In this case, the choice of initial phases and frequencies leads to a coherent state with $r \approxeq 1$ after integrating the system for a sufficiently long time. Then, we follow the same procedure as in the forward process but, after integrating the system for $T = 1500$, the value of K is decreased by $\delta K = 0.01$ until $K = 0.01$.

To provide a more refined description of collective states (compared to the global description provided by the order parameter), we use the mean frequency $\langle\omega_j\rangle = \langle\dot{\theta}_j\rangle$ of each oscillator, computed over the interval from $t = 1000$ to $t = 1500$ for each value of K. It is worth pointing out here that for each oscillator, we have defined three different frequencies: the natural frequency Ω_j, the (instantaneous) frequency $\omega_j = \dot{\theta}_j$, and the mean frequency $\langle\omega_j\rangle$.

Two oscillators are *synchronized* (or *frequency locked*) if they have the same mean frequency. A group of oscillators with the same value of mean frequency forms a *synchronized cluster*.

We compute the forward and backward process for three values of inertia: $m = 2$, $m = 5$, and $m = 10$. The results of the simulations are reported in Fig. 1.

We observe that for $m = 2$ in the forward process, we have a standard pathway to a coherent steady state in the sense that a main synchronized cluster is formed and gradually, as K increases, nearby oscillators are absorbed by the main cluster. Here, the value of the coherence r increases discontinuously at $K \approxeq 3.6$ [see Fig. 1(a)]. Moreover, Fig. 1(a) shows that throughout the forward process for each value of K the coherence is approximately constant. In the clustering diagram [Fig. 1(b)], we depict the mean frequency $\langle\omega_j\rangle$ of the oscillators as K increases. We observe that initially a synchronized cluster is abruptly formed at $K \approxeq 3.6$ around the peak of the distribution. Subsequently, nearby oscillators are gradually absorbed by the synchronized cluster leading to a more coherent state with larger r.

The dynamics of the order parameter for the system with $K = 4.8$ is shown in Figs. 2(a)–2(c). In Fig. 2(a), we observe that the evolution of the complex order parameter $r\,e^{i\phi}$ inside the unit disk on the complex plane takes place along a curve of constant radius r. This is also visible in Fig. 2(b). In Fig. 2(c), we depict the mean frequency $\langle\omega_j\rangle$ as a function of the natural frequency Ω_j. Note the appearance of a large main synchronized cluster with $\langle\omega\rangle = 0$ and the absence of any secondary synchronized clusters, in agreement with Fig. 1(b).

When the inertia is increased to $m = 5$, we no longer observe the same mechanism toward synchronization. The order parameter increases discontinuously at $K \approxeq 4.2$. However, in the resulting states, the value of r does not remain (approximately) constant but oscillates around a mean value. In Fig. 1(c), the mean value is depicted by the blue thick line while the width of the oscillation

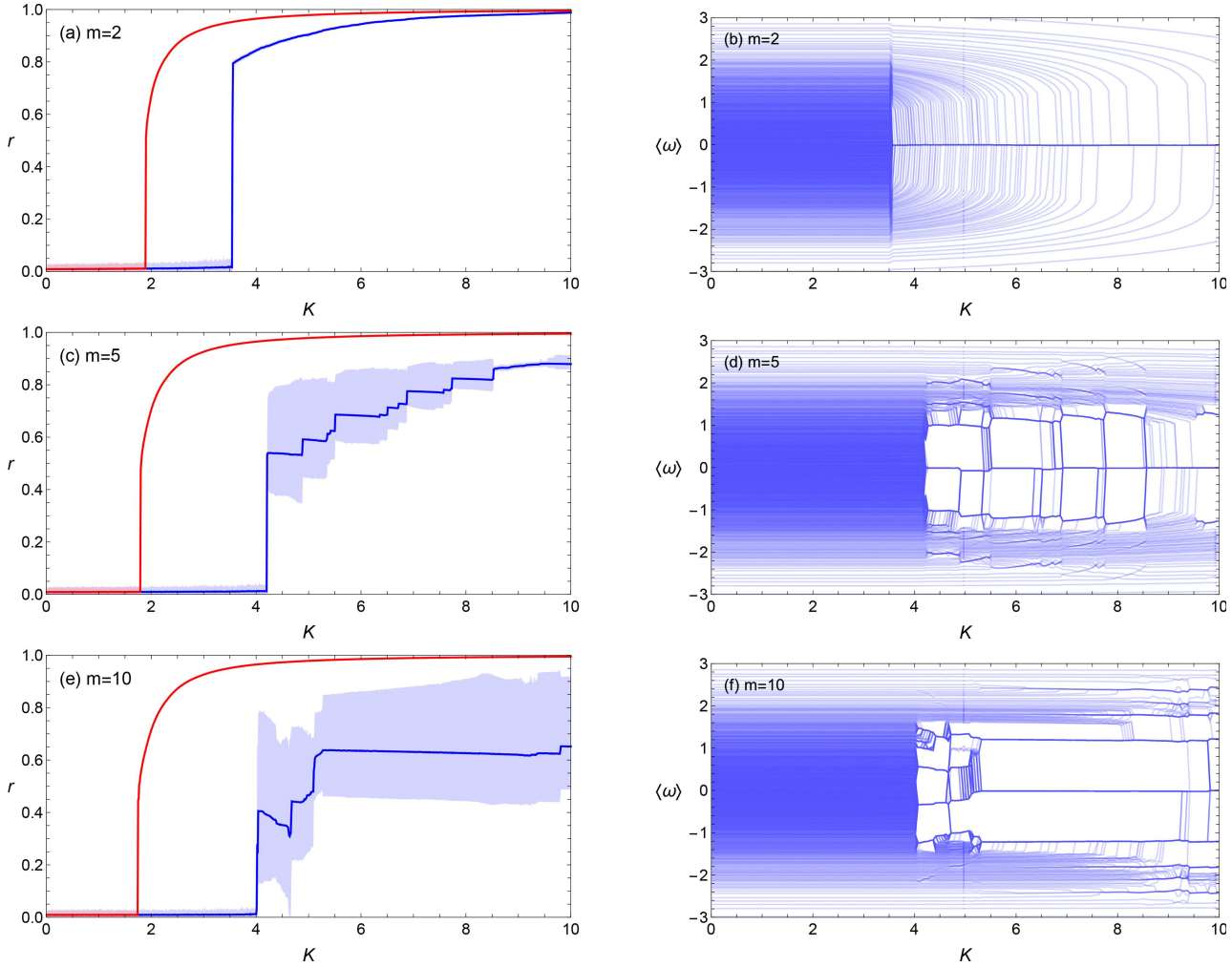

FIG. 1. Results of the numerical simulations for the forward and backward processes for $N = 10\,000$ oscillators and Gaussian natural frequency distribution $g_1(\Omega)$. The inertias considered in these pictures are $m = 2$ (top row), $m = 5$ (middle row), and $m = 10$ (bottom row). Left side: evolution of the coherence in the forward and backward processes described in the text. For each value of K, the mean coherence for the time interval from $t = 1000$ to $t = 1500$ is drawn with a thick blue curve for the forward process and a thick red curve for the backward process. The range of value of the coherence for each K is represented by the light blue band for the forward process and the light red band for the backward process. Right side: clustering diagrams show the mean frequency $\langle\omega_j\rangle$ for the time interval from $t = 1000$ to $t = 1500$ as K increases in the forward process. The successive merging of lines indicates the formation of synchronized clusters.

is represented by the light blue band around the mean value. In previous studies, this state has been called *secondary synchronization* (Tanaka *et al.*, 1997b) or *oscillatory state* (Olmi *et al.*, 2014 and Olmi and Torcini, 2016). Such an oscillatory state obtained from this forward process at $K = 4.8$ is depicted in Figs. 2(d)–2(f). In Fig. 2(d), we observe that the complex order parameter oscillates in the radial direction [see also Fig. 2(e)], while the collective phase ϕ also changes.

In the corresponding clustering diagram in Fig. 1(d), we observe that many smaller synchronized clusters are formed due to inertia alongside the main synchronized cluster that originates from the peak of the distribution. The clusters for $K = 4.8$ are depicted in Fig. 2(f), where we observe that the system has a main synchronized cluster with $\langle\omega\rangle = 0$, two relatively large secondary synchronized clusters symmetrically positioned with respect to 0, and even smaller synchronized clusters further away. As K increases, the main synchronized cluster becomes more prominent with oscillators from neighboring clusters gradually feeding into it. This leads to an increase of the coherence and a suppression of the oscillatory behavior.

The existence of the secondary synchronized clusters also explains the oscillatory behavior of the complex order parameter. To simplify the discussion, assume that $a_0 N$ oscillators are fixed at $\theta = 0$, $\frac{1}{2}a_1 N$ oscillators rotate as $\theta_i = \Omega_1^r t$ and $\frac{1}{2}a_1 N$ oscillators

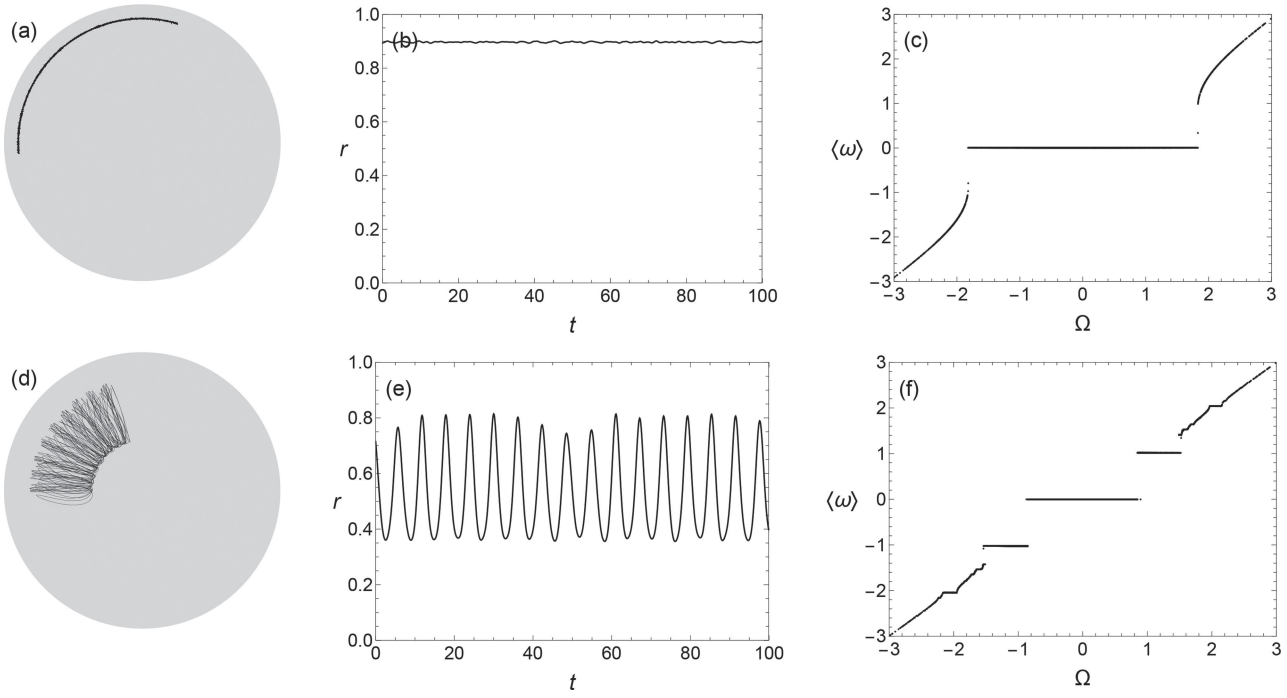

FIG. 2. Two states obtained from the forward process for the unimodal distribution $g_1(\Omega)$. At the leftmost panel, we depict the evolution of the order parameter $re^{i\phi}$ in the unit disk for the time interval from $t = 1000$ to $t = 1500$. In the middle panel, we depict the time-dependence of r from $t = 1000$ to $t = 1100$ sampled every $\Delta t = 0.1$. The rightmost panel shows the mean frequency $\langle\omega_j\rangle$ of the jth oscillator in the time interval from $t = 1000$ to $t = 1500$ as a function of the natural frequency Ω_j. Top row: a coherent steady state for $m = 2$ and $K = 4.8$; bottom row: an oscillatory state for $m = 5$ and $K = 4.8$.

rotate as $\theta_i = -\Omega_1^r t$, with $a_0 + a_1 = 1$. Then, the complex order parameter is

$$r\,e^{i\phi} = a_0 + \frac{a_1}{2}\left(e^{i\Omega_1^r t} + e^{-i\Omega_1^r t}\right) = a_0 + a_1\cos\Omega_1^r t, \tag{4}$$

which agrees with the definition of oscillatory states.

Further increasing the inertia to $m = 10$ makes the oscillatory behavior even more pronounced and we observe that it persists for all the range of K values that we have considered in our computations [see Fig. 1(e)], even though it is known that for sufficiently large values of K the system will reach a stationary state (Olmi *et al.*, 2014). Moreover, we observe that the mean value of the coherence remains almost constant for a large range of K, from $K \approxeq 5.2$ to $K \approxeq 9.8$. In the clustering diagram in Fig. 1(f) we observe a complex clustering process taking place from $K \approxeq 4.4$ to $K \approxeq 5.2$ before the system settles to three large synchronized clusters. Note that in all cases, the system will reach for sufficiently large K a stationary (non-oscillatory) partially coherent state; however, we do not show this transition for all simulations since we focus on the formation of secondary synchronized clusters.

In summary, these numerical calculations demonstrate that the main effect of inertia is to impede the formation of coherent stationary states by inducing the formation of secondary synchronized clusters. Note also that in the backward process, there are no oscillatory states in any of the numerical simulations.

Similar to the calculations in this section for a unimodal natural frequency distribution, we can further consider bimodal distributions. As we discuss in the Appendix, the role of inertia in this case is also to support the formation of secondary synchronized clusters.

III. TIME-PERIODIC MEAN FIELD

The dynamics described by Eq. (1) can be written in mean field form (Kuramoto, 1975), where each oscillator interacts with the mean field through the order parameter $z(t) = r(t)\,e^{i\phi(t)}$, as

$$\dot\theta_j = \omega_j, \tag{5a}$$

$$m\dot\omega_j + D\omega_j = \Omega_j + Kr(t)\sin(\phi(t) - \theta_j). \tag{5b}$$

Written in this form, the dynamical equations connect two levels of description of the system—the macroscopic description given by the order parameter $z(t)$ to the microscopic description given by the solutions $(\theta_j(t), \omega_j(t))$ for individual oscillators $j = 1, \ldots, N$. The essence of the self-consistent method is the fact that for a prescribed order parameter $z(t)$, the obtained solutions $(\theta_j(t), \omega_j(t))$ must satisfy

$$z(t) = \frac{1}{N}\sum_{j=1}^{N}\exp(i\theta_j(t)), \tag{6}$$

that is, the prescribed order parameter should equal the order parameter obtained by considering the solutions $(\theta_j(t), \omega_j(t))$ for the individual oscillators. Equation (6) can be viewed as connecting the microscopic to the macroscopic description, that is, its role is the reverse of the role of Eq. (5). If the solutions $(\theta_j(t), \omega_j(t))$ of Eq. (5) obtained with a prescribed $z(t)$ satisfy Eq. (6), then we can conclude that the prescribed $z(t)$ corresponds to a state that can be realized in the system. Such a state can be numerically observed if it is stable.

A. Dynamics in periodic mean field

Even though a self-consistent method for non-stationary states does not exist, understanding the dynamics induced by Eq. (5) for a prescribed oscillatory order parameter $z(t)$ allows us to reach important conclusions about the existence of secondary synchronized clusters in the systems under study.

For first-order Kuramoto oscillators, that is, $m = 0$, this idea was pursued by Engelbrecht and Mirollo (2012). In this case, the mean field equation under the assumption of a periodically varying order parameter gives rise to a time-dependent first-order equation with periodically varying coefficients. The Poincaré map for such an equation is a strictly increasing function of the phase θ, and, therefore, it gives rise to a circle map lift. The resulting rotation number is an increasing function of the natural frequency. The analysis of the rotation number shows the existence of synchronized clusters which manifest as plateaus for the rotation number, cf. the numerical results in Sec. II.

For the unimodal natural distribution, we can model the collective phases as $\phi(t) = \Omega^r t$, and the order parameter with the ansatz

$$r(t) = r_0 + \frac{r_1}{2} e^{i\Omega_1^r t} + \frac{r_1}{2} e^{-i\Omega_1^r t} = r_0 + r_1 \cos(\Omega_1^r t). \tag{7}$$

The ansatz in Eq. (7) gives $r(t)$ as the sum of contributions from a main synchronized cluster and drifting oscillators and two symmetric secondary synchronized clusters with frequencies $\pm\Omega_1^r$, cf. Eq. (4). Note that $r_1 = 0$ corresponds to a stationary states. We further discuss the validity of this ansatz in Sec. III C. Equation (7) belongs to a more general form as

$$r(t) = r_0(1 + \varepsilon f(t)), \tag{8}$$

with collective phase $\phi(t) = \Omega^r t + \phi_0$ with a constant precession rate Ω^r. Here, $f(t)$ is a T-periodic function, $T = 2\pi/\Omega_1^r$, with zero average and normalized so that $\max|f(t)| = 1$, while $\varepsilon \geq 0$ measures the relative size of the time-dependent term.

From Eq. (8), the dynamics of oscillators in Eq. (5) can be written in a frame rotating together with $\phi(t)$ as

$$\dot\theta = \omega, \tag{9a}$$

$$m\dot\omega + D\omega = \Omega - D\Omega^r - Kr_0(1 + \varepsilon f(t))\sin(\theta), \tag{9b}$$

where we have dropped the subscript j for individual oscillators.

We want to understand the dynamics of a single oscillator following Eq. (9) for ε close to 0, i.e., for near-stationary states. For a given initial state $(\theta(0), \omega(0))$, we consider the corresponding solution $(\theta(t), \omega(t))$ of Eq. (9). Then, the time-T Poincaré map $\widehat{F}$ on $\mathbb{R}^2$ corresponding to Eq. (9) is defined by

$$\widehat{F}: \mathbb{R}^2 \to \mathbb{R}^2 : (\theta(0), \omega(0)) \mapsto (\theta(T), \omega(T)). \tag{10}$$

Since θ is a periodic coordinate, we can define the corresponding Poincaré map F on the cylinder $C = \mathbb{S} \times \mathbb{R}$ by

$$F: C \to C : (\theta(0), \omega(0)) \mapsto (\theta(T) \bmod 2\pi, \omega(T)). \tag{11}$$

The case $\varepsilon = 0$ in Eq. (9) corresponds to a steady state with $r(t) = r_0$. We recall here some basic facts about the dynamics in this case—for more details, see Levi *et al.* (1978), Guckenheimer and Holmes (2013), Strogatz (2014), and Gao and Efstathiou (2018). The notation here follows (Gao and Efstathiou, 2018).

In the case $\varepsilon = 0$, Eq. (9) has two possible stable states. Let

$$a = \frac{D}{(Kr_0 m)^{1/2}}, \quad b = \frac{D\,\Delta\Omega}{Kr_0},$$

where $\Delta\Omega = (\Omega/D) - \Omega^r$. Then, for $b \geq b_L := 1$, the only stable state is a limit cycle L. The motion on L has the approximate period given by

$$T_L \approxeq \frac{2\pi}{\Delta\Omega},$$

i.e., it corresponds to an approximate average frequency $\Omega_L \approxeq \Delta\Omega$ on L. Note that a better estimate for Ω_L, valid for small Kr_0, is

$$\Omega_L \approxeq \Delta\Omega\left[1 - \frac{1}{2}\frac{(Kr_0)^2}{(D\,\Delta\Omega)^2 + \mu^2(D\,\Delta\Omega)^4}\right],$$

where $\mu = m/D^2$ is the reduced mass [see Gao and Efstathiou (2018)].

For $b < b_S(a)$, where

$$b_S(a) \approxeq \begin{cases} 1.2732\,a - 0.3056\,a^3, & 0 \leq a \leq 1.193, \\ 1, & a \geq 1.193, \end{cases} \tag{12}$$

the only stable state is a fixed point $(\theta_0, 0)$. When $b_S(a) < b < b_L := 1$ the system is *bistable*—the stable fixed point and stable limit cycle co-exist. Several properties of second-order oscillators, such as the discontinuous phase transitions to synchronization and the corresponding hysteresis of steady states, are closely related to this bistability.

To extend these results to the time-dependent system in Eq. (9) with $\varepsilon > 0$, consider the extended phase space $C \times \mathbb{S}_T$ with coordinates (θ, ω, t). Here, because of the periodic time-dependence of Eq. (9) on t, the latter is viewed as a periodic variable in $\mathbb{S}_T := \mathbb{R}/T\mathbb{Z}$, i.e., $t \in [0, T]$ with $0 \equiv T$. The stable fixed point $(\theta_0, 0)$ becomes in $C \times \mathbb{S}_T$ a stable limit cycle $(\theta_0, 0, t)$, or equivalently a fixed point $(\theta_0, 0)$ of the Poincaré map F. Similarly, the stable limit cycle L becomes in $C \times \mathbb{S}_T$ a stable limit torus $\widehat{L} = L \times \mathbb{S}_T$ carrying quasi-periodic motions with frequencies $2\pi/T_L$ and $2\pi/T$. The stable limit torus $\widehat{L}$ manifests on the Poincaré section as an invariant curve L_0 of

F carrying a quasi-periodic circle map with rotation number

$$\rho_0 = \frac{T}{T_L}.$$

Recall here that the rotation number for an orbit of the Poincaré map $\widehat{F}$ with initial state $(\theta(0), \omega(0))$ is

$$\mathrm{rot}(F)(\theta(0), \omega(0)) := \lim_{n\to\infty} \frac{\theta(nT) - \theta(0)}{2\pi n} = \lim_{n\to\infty} \frac{\theta_n - \theta_0}{2\pi n},$$

where $(\theta_n, \omega_n) = \widehat{F}^n(\theta(0), \omega(0))$.

Both the stable fixed point $(\theta_0, 0)$ and the stable invariant curve L_0 of F that exists for $\varepsilon = 0$ persist for sufficiently small $\varepsilon > 0$. In particular, the fixed point $(\theta_0, 0)$ of F persists as the fixed point $(\theta_\varepsilon, \omega_\varepsilon)$ from the general theory of persistence of equilibria (Guckenheimer and Holmes, 2013). Moreover, the invariant curve L_0 is a compact normally hyperbolic invariant manifold and thus Fenichel's theory (Hirsch *et al.*, 1970 and Fenichel, 1971) and we expect that for sufficiently small ε, it will persist as an invariant curve L_ε. Extending terminology from the case $\varepsilon = 0$, we will refer to oscillators converging to the stable fixed point as *locked* and those converging to the stable invariant curve as *running*, cf. Gao and Efstathiou (2018). The restriction of the Poincaré map F on the invariant curve L_ε gives rise to a circle map with a rotation number ρ_ε independent of the initial condition on the invariant curve (Devaney, 2003). Note that the circle map on L_ε may have fixed points or higher order resonances.

Consider now an ensemble of oscillators characterized by different Ω while the other parameters determining the dynamics, that is, m, D, K, r_0, Ω^r, ε and the T-periodic function $f(t)$ are the same. Then, the value of Ω determines whether the Poincaré map F for Eq. (9) for sufficiently small ε has a fixed point, an invariant curve, or both. Note here that for large ε, the Poincaré map F may also have other stable features (fixed points, invariant curves, or chaotic attractors).

Restricting our attention to the case of small ε if there is only a (stable) fixed point $(\theta_\varepsilon, \omega_\varepsilon)$, then all initial states $(\theta(0), \omega(0))$ will eventually converge to it and their rotation number will be $\mathrm{rot}(F)(\theta(0), \omega(0)) = 0$. Similarly, if there is only a stable invariant curve L_ε, then all orbits will have rotation number $\mathrm{rot}(F)(\theta(0), \omega(0)) = \rho_\varepsilon$. In the bistable case, where both a fixed point and an invariant curve co-exist, we will find some oscillators with rotation number 0 and some oscillators with rotation number ρ_ε depending on their initial condition $(\theta(0), \omega(0))$, which determines if they converge to the fixed point or the invariant curve, respectively. Therefore, a plot of $\mathrm{rot}(F)$ vs Ω for each oscillator will consist of three regions: one where all oscillators are running and have rotation number ρ_ε (which however depends on Ω), one where all oscillators are locked with rotation number 0, and the bistable region where some oscillators have rotation number 0 and some have rotation number ρ_ε.

B. Formation of secondary synchronized clusters

In Sec. II, we observed that secondary synchronized clusters appear only in the forward process and for sufficiently large inertias. Based on the dynamics of a single oscillator in a periodic mean field, we can now provide an explanation for this observation.

Figure 3 shows the rotation number of a single oscillator with dynamics given by Eq. (9) in an oscillatory mean field of the form $r(t) = r_0(1 + \varepsilon \cos t)$ for different values of inertia, fixed r_0, and gradually increasing ε. The parameter $\Delta\Omega = (\Omega/D) - \Omega^r$ ranges from $\Delta\Omega_{\min} = -3$ to $\Delta\Omega_{\max} = 3$ with step 10^{-2}. For each value of $\Delta\Omega$, we consider at least 10 randomly chosen initial conditions $(\theta(0), \omega(0))$ chosen uniformly in $[0, 2\pi] \times [-6, 6]$. For each initial condition, we numerically compute the rotation number by integrating the dynamics from $t = 0$ to $t = 2\pi \times 1200$ and then

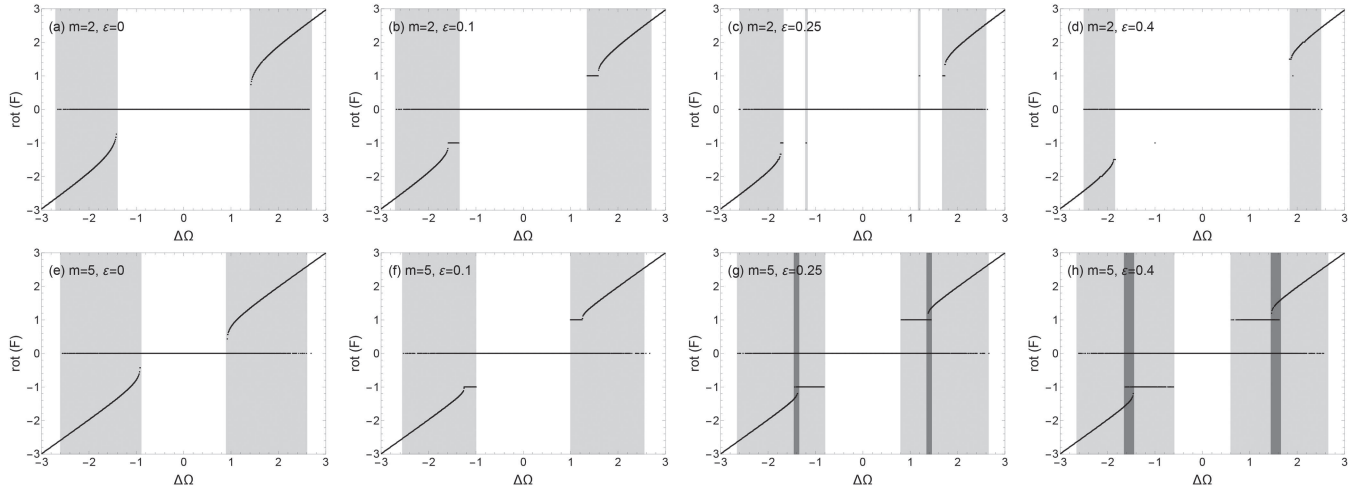

FIG. 3. Rotation number $\mathrm{rot}(F)$ as a function of $\Delta\Omega = (\Omega/D) - \Omega^r$ for Eq. (9) with oscillatory $r(t) = r_0(1 + \varepsilon \sin t)$. Top row: $m = 2$; bottom row: $m = 5$. The value of ε increases from left to right taking the values $\varepsilon = 0, 0.1, 0.25, 0.4$. In all cases, $D = 1$, $K = 4.5$, and $r_0 = 0.6$. Bistable regions are colored light gray, and multistable regions (three or more stable features) are colored dark gray.

numerically approximating the rotation number as

$$\mathrm{rot}(F) \approxeq \frac{1}{2\pi \times 1000}(\theta(2\pi \times 1200) - \theta(2\pi \times 200)).$$

In all computations, we have chosen $D = 1$, $K = 4.5$, and $r_0 = 0.6$.

For $m = 2$, we observe in Fig. 3(a) that for $\varepsilon = 0$ we have, depending on the value of $\Delta\Omega$, a stable fixed point (points on the plateau $\mathrm{rot}(F) = 0$) or a stable invariant curve (points outside the plateau)—these co-exist in the light gray colored bistable regions. For non-zero but small $\varepsilon = 0.1$, we observe in Fig. 3(b) that the numerical results agree with the theoretical analysis based on Fenichel's theory. In particular, the fixed points and the invariant curve persist. However, we also note that for a small range of values of the parameter $\Delta\Omega$ the appearance of resonances at $\mathrm{rot}(F) = \pm 1$ on the invariant curve and inside the bistable region. For even larger values $\varepsilon = 0.25$ in Fig. 3(c) and $\varepsilon = 0.4$ in Fig. 3(d), the resonances disappear.

For larger inertia $m = 5$, the dynamics of the system is very different. We observe in Figs. 3(e)–3(h) that as ε increases, the bistable region remains prominent—at $\varepsilon = 0.4$, we also observe the appearance of a multistable region. At the same time, as ε increases, the size of the resonances also increases.

The crucial observation here is that with increased inertia, we have larger plateaus in the graph of $\mathrm{rot}(F)$ vs Ω (corresponding to synchronized clusters) and these plateaus appear inside the bistable regions, as shown in Fig. 3. With a larger bistable region and corresponding larger plateaus, the time-periodic mean field can excite a larger oscillation of the order parameter. Taking the time-periodic mean field as an oscillating perturbation around stationary states, a sufficient large excited oscillation of the order parameter means the instability of such stationary state and the formation of an oscillatory state.

This observation explains why oscillatory states do not appear for small inertias or in the backward process. For oscillatory states to appear, it is necessary to have oscillators that will belong to one of the (secondary) plateaus besides the main plateau at $\mathrm{rot}(F) = 0$ since the latter corresponds to fixed points and contributes to the coherent stationary state. Since for small inertias these secondary plateaus are small, we do not expect that they will lead to the formation of oscillatory states. For large inertias, the plateaus increase in size but they are located inside the bistable region. This implies that they are accessible to oscillators in the forward process but inaccessible to oscillators in the backward process.

C. Initial states and self-consistency

For second-order Kuramoto oscillators, i.e., with $m > 0$, the initial state of the oscillators may lead to different final states after a transient time, due to bi-stability. For example, the numerical results in Sec. II demonstrate that, for sufficiently large m, one can find secondary synchronized clusters in the forward process but not in the backward process. The only difference between these two processes for a given coupling strength K is the initial state.

To explore the relation between initial states and secondary synchronized clusters, we fix K and we consider initial states parameterized by $\lambda \in [0, 1]$, where the initial phases $\theta_j(0)$ are randomly drawn from the uniform distribution with support in $[-\lambda\pi, \lambda\pi]$, and the initial frequencies $\omega_j(0)$ are randomly drawn from the uniform distribution with support in $[-\lambda, \lambda]$. When $\lambda = 0$, the initial state is a fully phase synchronized state with $r(0) = 1$. Such a state is always transient and evolves to a different final state. When $\lambda = 1$, the initial state is an incoherent state with $r(0) = 0$. In this case, the system can stay in the incoherent state if the state is stable and will evolve to a different final state if the incoherent state is unstable.

For the numerical simulations, we fix the parameters $m = 5$, $D = 1$, and $K = 5$. For each initial state, we let the system evolve for time $t = 4500$ and then fit the numerically computed coherence $r(t)$ from $t = 4500$ to $t = 5000$ to the ansatz $r(t) = r_0 + r_1 \cos(\Omega_1^r t)$ in Eq. (7) to obtain the values of the parameters r_0, r_1, Ω_1^r.

The results of the fitting for different initial states are shown in Fig. 4, where λ takes values from 0 to 1 with step 0.05, and for each λ, we have considered 10^3 random initial states. As an example, Fig. 4(a) shows the fitted $r(t)$ with $r_0 = 0.66$, $r_1 = 0.14$, and $\Omega_1^r = 1.12$ for $\lambda = 1$. Figures 4(b) and 4(c) show the fitted parameters r_0, r_1, and Ω_1^r for all λ and all initial states. We observe a clear separation in two clusters. One cluster has $r_1 < 0.015$ and corresponds to (near-)stationary states. The second cluster has $r_1 > 0.1$ and corresponds to oscillatory states, that is, states with prominent secondary synchronized clusters. Note that due to the random character of the initial states, it is possible that different initial states for the same λ give final states in different clusters. This is shown in Figs. 4(d)–4(f) where the fitted parameters for each initial state are shown as a function of λ. In particular, in Fig. 4(e), we observe that oscillatory states appear for $\lambda \geq 0.9$.

Partial synchronization states with a constant order parameter $r(t) \approxeq r_0$ (in the cluster with $r_1 < 0.015$), can be analyzed using the self-consistent method.

Figures 4(b) and 4(c) show that for oscillatory states with secondary synchronized clusters, there is a linear relation between the three parameters r_0, r_1, and Ω_1^r. We observe that as r_1 increases, r_0 and Ω_1^r both linearly decrease. This implies that the parameters for the observed oscillatory states satisfy specific constraints. Such constraints can be uncovered through a detailed analysis of the dynamics of Eq. (9) with prescribed order parameter in Eq. (7). Combined with the self-consistent analysis, this could lead to the theoretical prediction of possible oscillatory states and the values of r_0, r_1, Ω_1^r as functions of K. Due to the extensive scope of this analysis, we do not further pursue this line of research here.

A related question is whether the order parameter obtained by considering the dynamics of individual oscillators in a prescribed mean field $r(t) = r_0 + r_1 \cos(\Omega_1^r t)$ is consistent with the given mean field. In particular, we consider the mean field $r_*(t) = 0.66 + 0.14 \cos(1.12\, t)$ given by the fitting for $\lambda = 1$ shown in Fig. 4(a) for $m = 5$, $D = 1$, and $K = 5$. In Fig. 5, we show the average frequency $\langle\omega\rangle$ of oscillators following the dynamics in Eq. (9) with the prescribed $r_*(t)$. The natural frequency Ω takes values from -4 to 4 with step 0.1. For each value of Ω, $N = 1000$ oscillators are considered with randomly chosen initial states. In Fig. 5(a), we observe the existence of the main synchronized cluster (A_2) corresponding to fixed points $(\theta_\varepsilon, \omega_\varepsilon)$ of the Poincaré map, and the secondary synchronized clusters (A_1) corresponding to fixed points of the circle map induced on the invariant curve L_ε, cf. the discussion in Sec. III A. Moreover, we observe the existence of drifting oscillators that correspond to non-resonant dynamics of the circle map on L_ε.

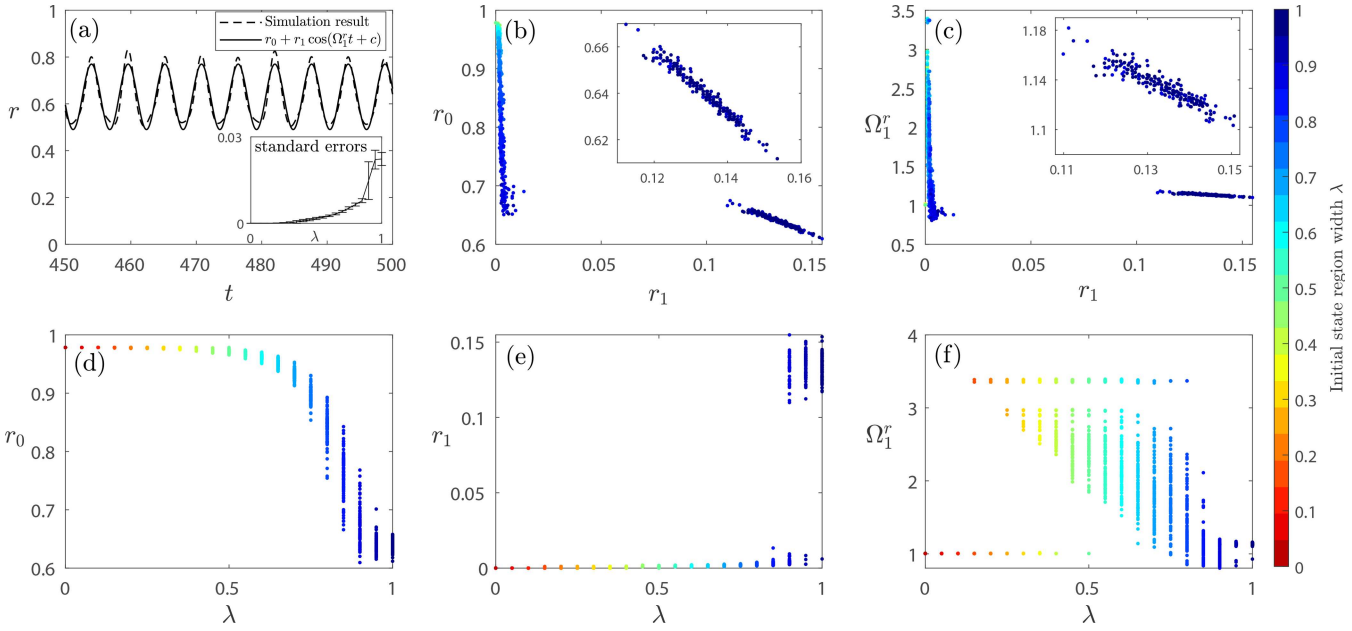

FIG. 4. (a) The order parameter $r(t)$ and the fit from Eq. (7) for one initial state with $\lambda = 1$. The inset shows the error of the fitting. (b) Fitted values r_0 vs r_1; the inset shows oscillatory states. (c) Fitted values Ω_1^r vs r_1; the inset shows oscillatory states. (d)–(f) Values of fitted parameters r_0, r_1, Ω_1^r, respectively, vs λ. In all simulations, $N = 10^3$, $m = 5$, $D = 1$, and $K = 5$. The natural frequencies Ω_j are drawn from the Gaussian distribution $g_1(\Omega)$. The initial states are drawn from $\theta_j(0) \in [-\lambda\pi, \lambda\pi]$ and $\omega_j(0) \in [-\lambda, \lambda]$, where $\lambda \in [0, 1]$ with a step 0.05. Simulation parameters are $dt = 0.01$ with $t \in [0, 5000]$. Equation (7) is fitted to $r(t)$ for $t \in [4500, 5000]$.

In Fig. 5(b), we show the basins of attraction for the states A_1 (gray) and A_2 (black) for $\Omega = 1.2$ [vertical dashed line in Fig. 5(a)]. The complicated shapes of the two basins highlight the difficulty of the detailed analysis of the dynamics produced by Eq. (9) and further demonstrate the bistability of the system.

Finally, in Fig. 5(c), we consider $N = 10^3$ oscillators with natural frequency Ω drawn from the distribution $g_1(\Omega)$ and random initial states with $\theta(0) \in [-\pi, \pi]$ and $\omega(0) \in [-4, 4]$. We integrate the oscillators from $t = 0$ to $t = 1000$ in the mean field $r_*(t)$ and use the obtained phases $\theta_j(t)$ to compute the order parameter $r(t) = 1/N \sum_j \exp(i\theta_j(t))$. We fit the ansatz $r_0 + r_1 \cos(\Omega_1^r t)$ to the computed order parameter $r(t)$ from $t = 500$ to $t = 1000$, obtaining the fitted values for r_0, r_1, and Ω_1^r. We repeat the process 10^5 times with different randomly chosen initial conditions. In Fig. 5(c), we

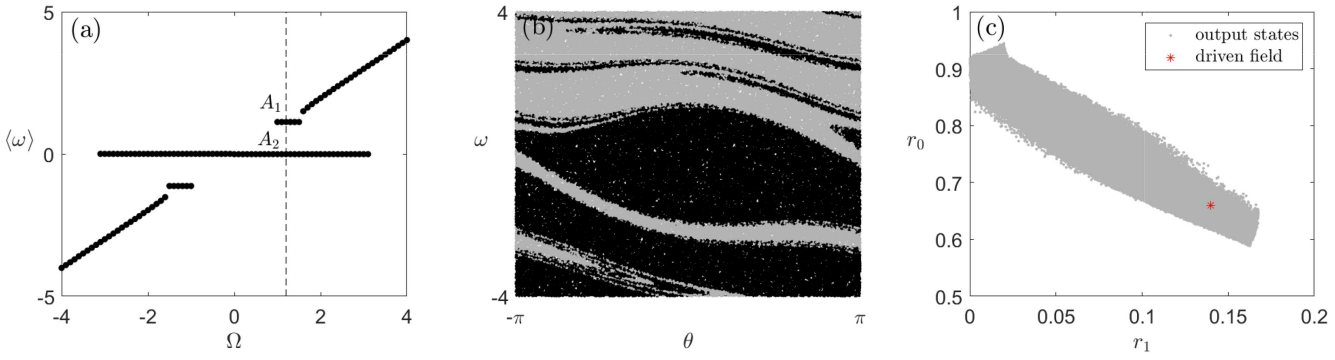

FIG. 5. Oscillator dynamics in the prescribed mean field $r_*(t) = 0.66 + 0.14\cos(1.12\,t)$. (a) Mean frequencies $\langle\omega\rangle$ of oscillators of Eq. (7), with $\Omega \in [-4, 4]$ with a step 0.1. For each value of Ω, $N = 1000$ oscillators are considered whose initial states are chosen randomly from $\theta(0) \in [-\pi, \pi]$ and $\omega(0) \in [-4, 4]$. (b) Basins of attraction for the state A_1 (gray) and A_2 (black) obtained by integrating $N = 10^5$ initial states. (c) The region of possible output states (gray points) and the driven field (red asterisk). The region of possible output states is obtained by integrating $N = 10^5$ randomly chosen initial states. The parameters calculated in (c) is $r_0 \in [0.5, 0.8]$ with step 0.03, and $r_1 \in [0.08, 0.18]$ with step 0.01. Simulation parameters are $m = 5$, $D = 1$, $K = 5$, and $dt = 0.01$ with $t \in [0, 1000]$. All fittings are for the time period $t \in [500, 1000]$.

show the obtained values of r_0 and r_1. We observe that these cover a region in the (r_1, r_0) plane and the mean field $r_*(t)$ lies inside this region. This implies that there are initial conditions that lead to the prescribed mean field $r_*(t)$, that is, the latter is consistent with the dynamics of the system. This confirms the validity of modeling the oscillatory mean field $r(t)$ using the ansatz $r_0 + r_1 \cos(\Omega_1^r t)$.

IV. MINIMAL MODEL FOR SECONDARY SYNCHRONIZED CLUSTERS

As a complement to the mean field based analysis in Sec. III, this section is devoted to the dynamics of a few oscillators as a simple model that demonstrates the role of inertia in the formation of secondary synchronized clusters.

Our approach here is a specific instance of the more general idea that dynamical phenomena in complex systems can be understood by constructing a simplified version of the original system that exhibits similar phenomena and is easier to analyze. For example, star networks have been used to demonstrate the main features of explosive synchronization (Gómez-Gardeñes *et al.*, 2011), while similar simplified models, including a four oscillator model, have been used to study weak chimera states (Ashwin and Burylko, 2015) and blinking chimeras (Goldschmidt *et al.*, 2019). Following established terminology (Ashwin and Burylko, 2015), we call such a simplified model a minimal model.

Note that a minimal model is not designed to be equivalent to the full original system but to capture the dynamical features of interest. For the role of inertia in the appearance of secondary synchronized clusters, the minimal model we consider is a coupled three-oscillator system. To create this minimal model, our starting point is the observation that since all oscillators in Eq. (1) are connected to each other, there is no topological effect and the only factor that affects the synchronization process is the natural frequency distribution $g(\Omega)$. We thus consider a system where the oscillators follow a discrete natural frequency distribution. That is, the N oscillators are grouped into N_G groups so that the ith group contains $w_i N$ oscillators with natural frequency Ω_i. Moreover, we assume that the oscillators in the ith group are phase and frequency synchronized with common phase θ_i and common frequency ω_i.

Then, the dynamics for an oscillator in the ith group is given by

$$\dot{\theta}_i = \omega_i,$$

$$m\dot{\omega}_i + D\omega_i = \Omega_i + K\sum_{j=1}^{N_G} w_j \sin(\theta_j - \theta_i).$$

In terms of a second-order equation, we have

$$m\ddot{\theta}_i + D\dot{\theta}_i = \Omega_i + K\sum_{j=1}^{N_G} w_j \sin(\theta_j - \theta_i). \tag{13}$$

The last equation can be viewed as describing N_G weighted oscillators with w_i being the weights. Thus, the original system of N oscillators is replaced by a smaller system of N_G weighted oscillators.

To demonstrate the effect of inertia to the formation of secondary synchronized clusters we consider, as previously mentioned, the case of three-coupled oscillators and we assign weights $w_0 \gg w_1 > w_2$ and natural frequencies 0, Ω, and $\Omega + \Delta\Omega$ with $\Omega \gg \Delta\Omega$. Oscillator 0 is assigned the largest weight w_0, describing the main synchronized cluster, and oscillators 1 and 2 are assigned smaller weights w_1 and w_2 but closer natural frequencies, describing two small synchronized clusters away from the main one [see Fig. 8(a)]. The benefit of considering such a minimal model is that the effect of inertia can be analyzed theoretically.

Introducing the phase differences $\varphi_1 = \theta_1 - \theta_0$, $\varphi_2 = \theta_2 - \theta_1$, we rewrite the dynamics as

$$m\ddot{\varphi}_1 + D\dot{\varphi}_1 = \Omega - K\left[A\sin(\varphi_1) - w_2\sin(\varphi_2) + w_2\sin(\varphi_1 + \varphi_2)\right], \tag{14a}$$

$$m\ddot{\varphi}_2 + D\dot{\varphi}_2 = \Delta\Omega - K\left[\Delta A\sin(\varphi_2) - w_0\sin(\varphi_1) + w_0\sin(\varphi_1 + \varphi_2)\right], \tag{14b}$$

where $A = w_0 + w_1$ is the combined weight of oscillators 0 and 1, and $\Delta A = w_2 + w_3 \ll A$ is the combined weight of oscillators 1 and 2.

Even though the system in Eq. (14) has various dynamical properties, we are only interested in the synchronization of each pair of oscillators. Since $A \gg w_2$, we can ignore in Eq. (14a) the perturbations from φ_2 and obtain the equation

$$m\ddot{\varphi}_1 + D\dot{\varphi}_1 = \Omega - KA\sin(\varphi_1), \tag{15}$$

which describes the synchronization between oscillators 0 and 1. The dynamics in Eq. (15) are the same as the dynamics of a single second-order oscillator (Levi *et al.*, 1978 and Gao and Efstathiou, 2018). The synchronization condition, $\dot{\varphi}_1 = 0$, can be written as

$$\frac{\Omega}{KA\, b_P\left(\frac{1}{\sqrt{K\mu A}}\right)} = \frac{\mu\Omega}{\beta(K\mu A)} \leq 1, \tag{16}$$

where we have defined

$$\beta(x) = x\, b_P\left(\frac{1}{\sqrt{x}}\right),$$

and we recall that $\mu = m/D^2$ is the reduced mass.

The boundary function $b_P(x)$ equals either $b_S(x)$ or $b_L(x) \equiv 1$ in the forward and backward processes, respectively. In both cases, the function $\beta(x)$ is invertible—see Fig. 6 for the graph of $\beta^{-1}(x)$—and, therefore, we can solve Eq. (16) to determine the critical value K_1 for the synchronization of oscillators 0 and 1, given by

$$K_1 = \frac{\beta^{-1}(\mu\Omega)}{\mu A}. \tag{17}$$

For $K < K_1$, the system converges to a stable limit cycle with $\dot{\varphi}_1 \approxeq \omega_1 = \Omega/D$. Then, for the synchronization of the oscillators 1 and 2, we have

$$m\ddot{\varphi}_2 + D\dot{\varphi}_2 = \Delta\Omega - K\Delta A\sin(\varphi_2) + Kw_0\left[\sin(\varphi_2 + \omega_1 t) - \sin(\omega_1 t)\right].$$

Since Ω is large, we can average the fast periodic perturbation from φ_1 over time and obtain the averaged dynamics of φ_2 as

$$m\ddot{\varphi}_2 + D\dot{\varphi}_2 = \Delta\Omega - K\Delta A\sin(\varphi_2). \tag{18}$$

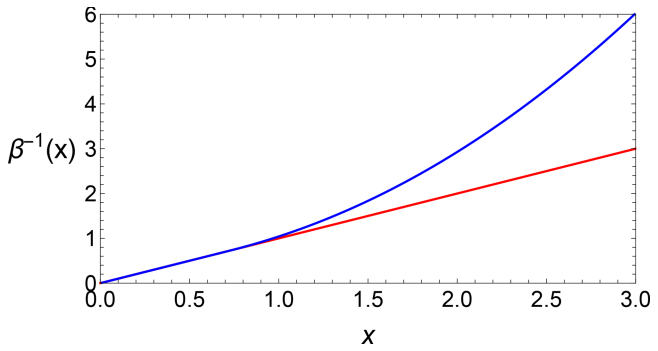

FIG. 6. The graph of $\beta^{-1}(x)$. The red curve represents the backward process, i.e., $b = b_L$, where $\beta^{-1}(x) = x$. The blue curve represents the forward process, i.e., $b = b_S$.

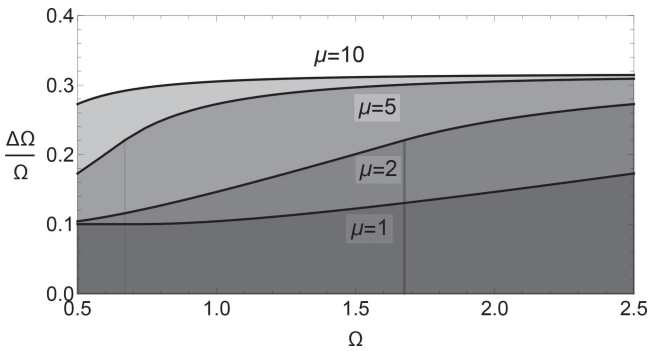

FIG. 7. Curves $C(\mu) = 1$ for $\Delta A/A = 0.1$ and $\mu = 1, 2, 5, 10$. The region $C(\mu) > 1$ corresponding to the synchronization of oscillators 1 and 2 lies below each curve.

Note that the last equation has the same form as Eq. (15) and, therefore, we can define a critical value

$$K_2 = \frac{\beta^{-1}(\mu\Delta\Omega)}{\mu\Delta A} \tag{19}$$

for the synchronization of oscillators 1 and 2.

Since in the backward process the function $b_L(x) \equiv 1$ is constant, we find $\beta^{-1}(x) = x$, and the transition process is independent of μ. In particular, the critical values of K are

$$K_1 = \frac{\Omega}{A}, \quad K_2 = \frac{\Delta\Omega}{\Delta A}.$$

In the forward process, with nonlinear boundary function $b_S(x)$, Eq. (12), the synchronization process depends on the value of μ. We define

$$C(\mu) = \frac{K_1}{K_2} = \frac{\Delta A}{A}\frac{\beta^{-1}(\mu\Omega)}{\beta^{-1}(\mu\Delta\Omega)}. \tag{20}$$

If $C(\mu) < 1$, oscillator 1 will first merge with oscillator 0 at $K_1 < K_2$ while if $C(\mu) > 1$ oscillator 1 will first merge with oscillator 2 at $K_2 < K_1$. The level sets $C(\mu) = 1$ in the $(\Omega, \Delta\Omega/\Omega)$ plane for fixed $\Delta A/A = 0.1$ and different values of μ are shown in Fig. 7. We observe that as μ increases, the region in which we theoretically predict that oscillators 1 and 2 will synchronize first also increases.

To better understand this phenomenon, we contrast the cases of small μ and large μ. Note that for small x, we have $\beta^{-1}(x) = x$, while for sufficiently large $x > 0.74$, we have $\beta^{-1}(x) \approxeq 0.48 + 0.62x^2$, cf. the graph of $\beta^{-1}(x)$ in Fig. 6. For $x \gg 1$, we approximate $\beta^{-1}(x) \sim x^2$. This implies that for small μ, we have

$$C_{\text{small }\mu} = \frac{K_1}{K_2} = \frac{\Omega}{\Delta\Omega}\frac{\Delta A}{A}.$$

However, for large μ such that $\mu\Omega \gg \mu\Delta\Omega \gg 1$, we have

$$C_{\text{large }\mu} = \frac{K_1}{K_2} \approxeq \left(\frac{\Omega}{\Delta\Omega}\right)^2 \frac{\Delta A}{A} = \frac{\Omega}{\Delta\Omega} C_{\text{small }\mu}.$$

Since $\Omega/\Delta\Omega \gg 1$, we conclude that even if for small μ, we have $C_{\text{small }\mu} < 1$ and oscillator 1 first merges with oscillator 0 (i.e., it joins the main cluster); for large μ, the process can be changed. In particular, if $\Omega/\Delta\Omega$ is large enough so that $C_{\text{large }\mu} > 1$, then oscillator 1 will merge with oscillator 2 to form a secondary cluster.

We conclude that for larger inertias, the oscillators are more likely to synchronize among ones with closer natural frequencies rather than with the main synchronized cluster. Consequently, we observe the appearance of additional synchronized clusters in the forward processes with sufficient large inertias.

In Fig. 8, we confirm through simulations the results of the theoretical analysis. We consider the forward process for three oscillators with $\Omega_0 = 0$, $\Omega_1 = 1$, $\Omega_2 = 1.15$ and $w_0 = 0.95$, $w_1 = 0.05$, $w_2 = 0.05$ [see Fig. 8(a)]. Therefore, $\Delta\Omega/\Omega = 0.15$ and $\Delta A/A = 0.1$. Then, $C_{\text{small }\mu} = 2/3 < 1$ and this implies that for small

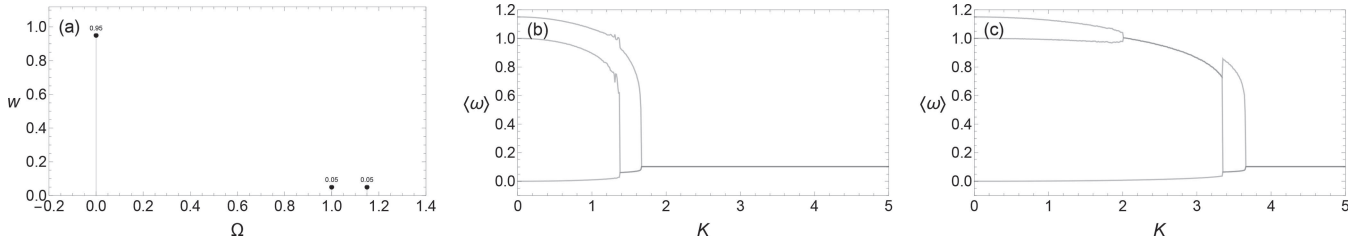

FIG. 8. (a) Weights w_i for oscillators with natural frequency Ω_i; (b) synchronization in the forward process with $m = 2$; and (c) synchronization in the forward process with $m = 5$.

$\mu = m/D^2$, oscillator 1 will first merge with oscillator 0 as shown in Fig. 8(b) where $m = \mu = 2$. However, for large μ, we have C_{large} $\mu = 40/9 > 1$ and this implies that for large μ, oscillator 1 will first merge with oscillator 2 as shown in Fig. 8(c) where $m = \mu = 5$. Note here that even though oscillators 1 and 2 synchronize, such synchronization is not perfect and it is possible for larger K to have oscillator 1 split off from the pair and synchronize with oscillator 0 as shown in Fig. 8(c). This does not contradict our theoretical analysis where we analyzed only the question of which oscillator pair will synchronize first and did not consider the full dynamics of the system.

Note that, as a generalization of these three-coupled oscillators, one can also consider three groups of oscillators as a limiting case of multimodal frequency distributions. This is beyond the scope of this paper and we refer to Acebrón and Bonilla (1998) and Acebrón *et al.* (2001).

V. DISCUSSION

In this paper, we analyzed the appearance of non-stationary states in the synchronization process of second-order oscillators and the role of inertia. The numerical results in Sec. II demonstrate that the role of inertia is to impede the formation of large synchronized clusters and to facilitate the creation of smaller, secondary, synchronized clusters. These secondary clusters, in turn, manifest through the macroscopic order parameter either as oscillations of the coherence or as standing waves.

In Sec. III, following the approach of Engelbrecht and Mirollo (2012), we considered the problem of an oscillator whose dynamics is determined by a mean field with oscillatory or standing wave coherence. We showed both numerically and theoretically that in these cases the graph of the rotation number as a function of the natural frequency has plateaus that correspond to synchronized clusters. Moreover, we numerically showed that the mean field description is consistent with the numerical results.

Finally, in Sec. IV, we considered a simplified minimal model with only three oscillators and we used it to understand how inertia affects synchronization. Our findings in this minimal model agree with the numerical results of Sec. II and reveal that large inertias can lead to the mutual synchronization of oscillators far from the main synchronized cluster.

One can see the results in Sec. III as one side of the self-consistent method. Starting with a periodic mean field, we analyzed the types of dynamics that oscillators can exhibit in this case. What is missing is a full self-consistent description of oscillatory and standing wave states. Such a self-consistent description of non-stationary states remains elusive even for standard Kuramoto oscillators and would be a major step forward in understanding non-stationary states in coupled oscillators.

ACKNOWLEDGMENTS

We acknowledge the Center for Information Technology of the University of Groningen for the use of the Peregrine HPC cluster. J. Gao acknowledges support by a China Scholarship Council (CSC) scholarship.

APPENDIX: BIMODAL NATURAL FREQUENCY DISTRIBUTIONS

In this appendix, we consider the effect of the distribution of natural frequencies to the formation of secondary synchronized clusters. In particular, instead of the unimodal distribution $g_1(\Omega)$ that we introduced in Sec. II, we consider here two bimodal natural frequency distributions.

The first bimodal distribution, having well separated modes, is given by

$$g_2(\Omega) = \frac{1}{2}G(\Omega; \tfrac{3}{2}, \tfrac{1}{2}) + \frac{1}{2}G(\Omega; -\tfrac{3}{2}, \tfrac{1}{2}). \tag{A1}$$

The second bimodal distribution is given by

$$g_3(\Omega) = \frac{1}{2}G(\Omega; 1,\ 0.7) + \frac{1}{2}G(\Omega; -1,\ 0.7). \tag{A2}$$

Here, the two modes are closer together and the separation between them is not as pronounced as for $g_2(\Omega)$ (see Fig. 9).

1. Phenomenology

The results of the numerical simulations for the forward and backward processes and for inertias $m = 2$, $m = 5$, and $m = 10$ for the distribution $g_2(\Omega)$ are shown in Fig. 10.

For $m = 2$, we observe in Fig. 10(a) that at $K \approxeq 2.9$ in the forward process, the mean coherence increases discontinuously but it is also combined with strong oscillations from $r = 0$ to some maximal value close to 1. Figure 10(b) shows that this is a result of the formation of two synchronized clusters at the two peaks of the natural frequency distribution. The corresponding state is shown in more detail in Fig. 11 for $K = 5.0$. We observe in Fig. 11(a) that the complex order parameter $re^{i\phi}$ combines a fast radial motion that passes very close to the origin with a slow angular precession. Plotting only the value of r as a function of t, we obtain the behavior shown in Fig. 11(b). We call such non-stationary state, a *standing wave state*.

In Fig. 11(c), we observe the existence of the two large synchronized clusters. The existence of these clusters also explains the particular behavior of the complex order parameter. In particular, and to simplify the discussion, assume that $N/2$ oscillators rotate as

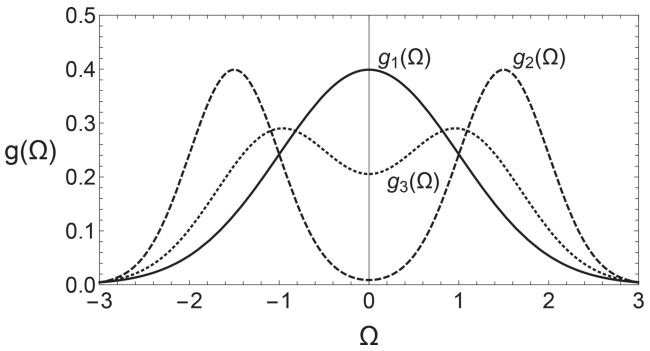

FIG. 9. Natural frequency distributions used in the numerical simulations in Sec. II and in the Appendix.

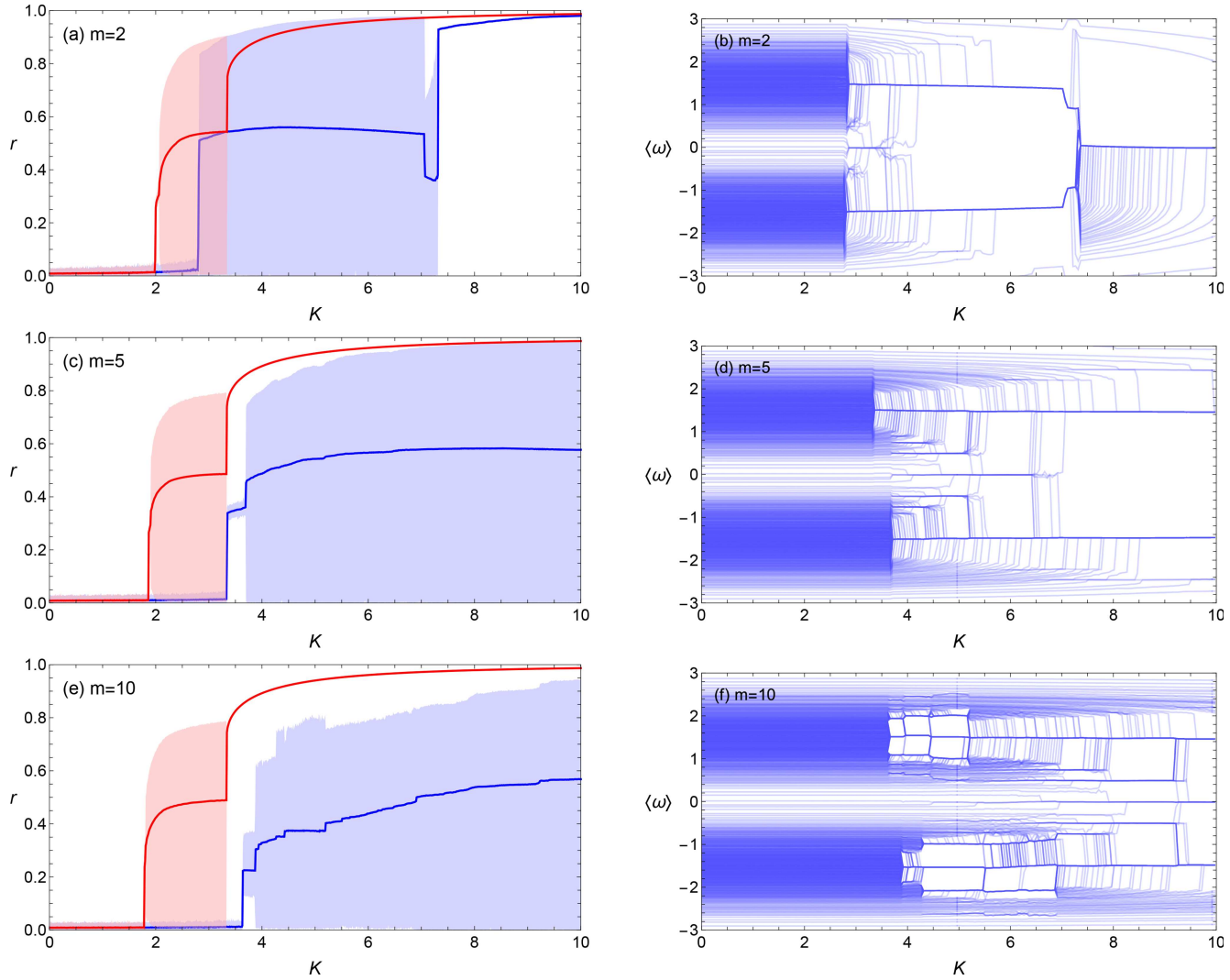

FIG. 10. Results of the numerical simulations for the forward and backward processes for $N = 10\,000$ oscillators and bimodal natural frequency distribution $g_2(\Omega)$ with clearly separated modes. The inertias considered in these pictures are $m = 2$ (top row), $m = 5$ (middle row), and $m = 10$ (bottom row). The description of the panels at the left and right sides is as in Fig. 1.

$\theta_i = \omega t$ while the other $N/2$ oscillators rotate as $\theta_i = -\omega t$. Then, the complex order parameter is

$$r\,e^{i\phi} = \frac{1}{2}(e^{i\omega t} + e^{-i\omega t}) = \cos\omega t, \tag{A3}$$

which agrees with our definition of a standing wave state. Note that in Olmi and Torcini (2016), a standing wave state is defined through the existence of two synchronized clusters with opposite frequencies.

As K further increases, we observe in Fig. 10(a) that the two synchronized clusters first shed some oscillators and then they merge and the system reaches a coherent stationary state.

In the backward process, we observe in Fig. 10(a) the appearance of standing waves when the coupling strength drops below $K \approxeq 3.4$. This contrasts with the unimodal case where there are no non-stationary states in the backward process.

For $m = 5$, we observe in Figs. 10(c) and 10(d) that one of the synchronized clusters associated with the two peaks of the natural frequency distribution is formed first and this induces a discontinuous increase of the coherence but no strong oscillatory behavior. This state has been called a traveling wave state in Olmi and Torcini (2016). When the synchronized cluster associated with the second peak is formed, then we obtain a standing wave state, which persists for K as large as 10. Again, we observe the formation of standing waves in the backward process.

Finally, for $m = 10$, we observe in Figs. 10(e) and 10(f), a much more complicated process of cluster formation where the

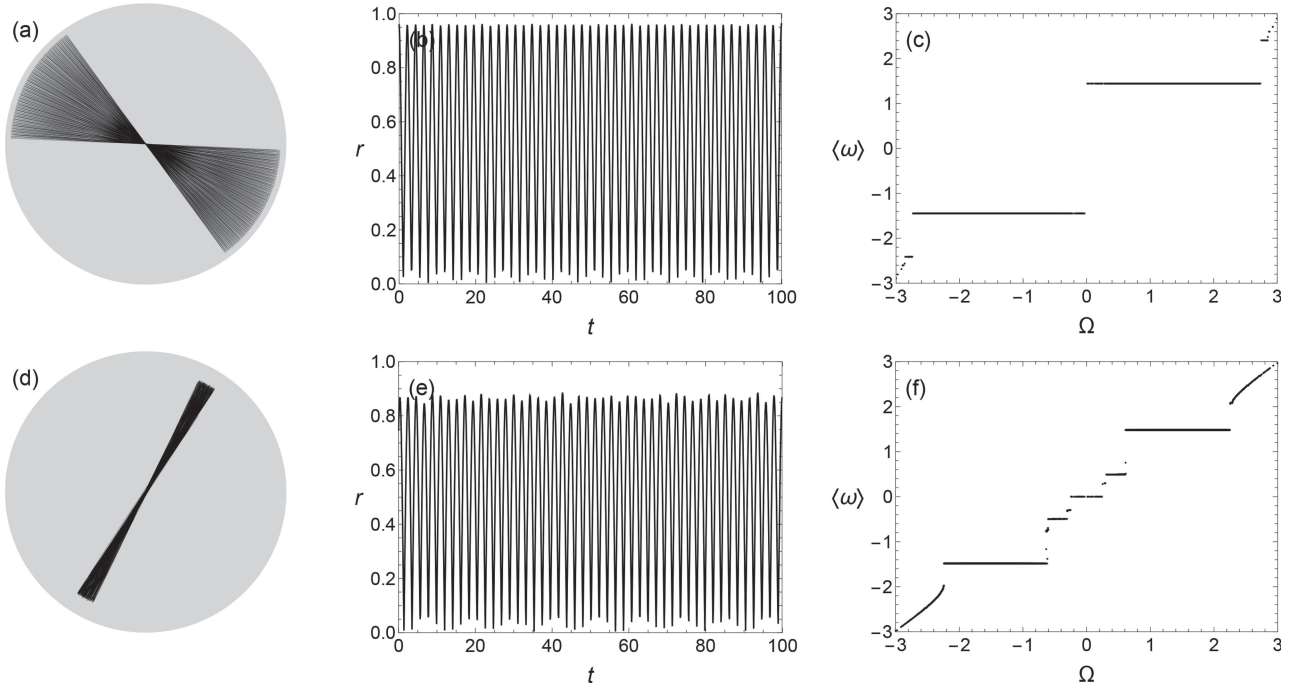

FIG. 11. States obtained from the forward process for the bimodal distribution $g_2(\Omega)$ with clearly separated modes. Top row: a standing wave state for $m = 2$ and $K = 5.0$; bottom row: a second standing wave state for $m = 10$ and $K = 8.0$. The description of the panels is as in Fig. 2.

synchronized clusters absorb but also shed oscillators. Note, in particular, the appearance of several secondary synchronized clusters except the two main synchronized clusters associated with the two peaks of the natural frequency distribution. One state for $K = 8.0$ is depicted in Figs. 11(d)–11(f). Figures 11(d) and 11(e) are similar to Figs. 11(a) and 11(b), respectively. However, in Fig. 11(f) and in agreement with Fig. 10(f), we clearly see the two main synchronized clusters associated with the two peaks of the natural frequency distribution together with some smaller secondary synchronized clusters. We also note the appearance of a traveling wave state from $K \approxeq 3.6$ to $K \approxeq 3.9$. In the backward process, we again have the appearance of standing wave states as the coupling strength gets smaller.

The last distribution we consider is the bimodal distribution $g_3(\Omega)$ with strongly overlapping modes. We expect that in this case, the behavior of the system will be a mixture of the behaviors for the unimodal case in Sec. II and the bimodal distribution $g_2(\Omega)$ in the present section. The results of the numerical simulations for the forward and backward processes and for inertias $m = 2$, $m = 5$, and $m = 10$ are shown in Fig. 12.

For $m = 2$, we observe in Figs. 12(a) and 12(b) that the system behaves very similarly to the corresponding unimodal case with $m = 2$.

For the intermediate value $m = 5$, we observe a much more complicated synchronization scenario with the formation of several clusters and the appearance of oscillatory states. In this case, the behavior is more similar to the corresponding unimodal case since we do not observe standing waves. However, if we look more closely at such an oscillatory state, Fig. 13(a), we observe that the precession of the order parameter is faster compared to the corresponding oscillatory state in the unimodal case in Fig. 2(d). Moreover, the synchronized clusters in the two cases have different structures as can be observed by comparing Figs. 13(c) to 2(f). Note also that, similar to the unimodal case, non-stationary states do not appear in the backward process.

Finally, for $m = 10$, we observe the creation of several small synchronized clusters, in agreement with our previous observations for large inertias. We observe that in this case, the bimodality becomes more apparent and this indicates that inertia here plays the role of enhancing the effect of bimodality. In particular, we observe the appearance of standing waves for coupling strength larger than $K \approxeq 5$. In this respect, this case should be compared to the corresponding case for the bimodal distribution $g_2(\Omega)$ in Figs. 10(e) and 10(f). However, non-stationary states do not appear in the backward process in contrast to all the numerical simulations for $g_2(\Omega)$. The standing wave state for $m = 10$ and $K = 8$ is shown in Figs. 13(d)–13(f) where we observe a more complicated pattern compared to the standing wave states in Fig. 11. In summary, the numerical results for bimodal distributions confirm that the role of inertia is to support the formation of secondary synchronized clusters. Moreover, the degree of the overlap of the two modes in the bimodal distribution controls the type of non-stationary states that appear. Small overlap favors the formation of standing wave states while large overlap, bringing the distribution closer to the unimodal case, favors oscillatory states.

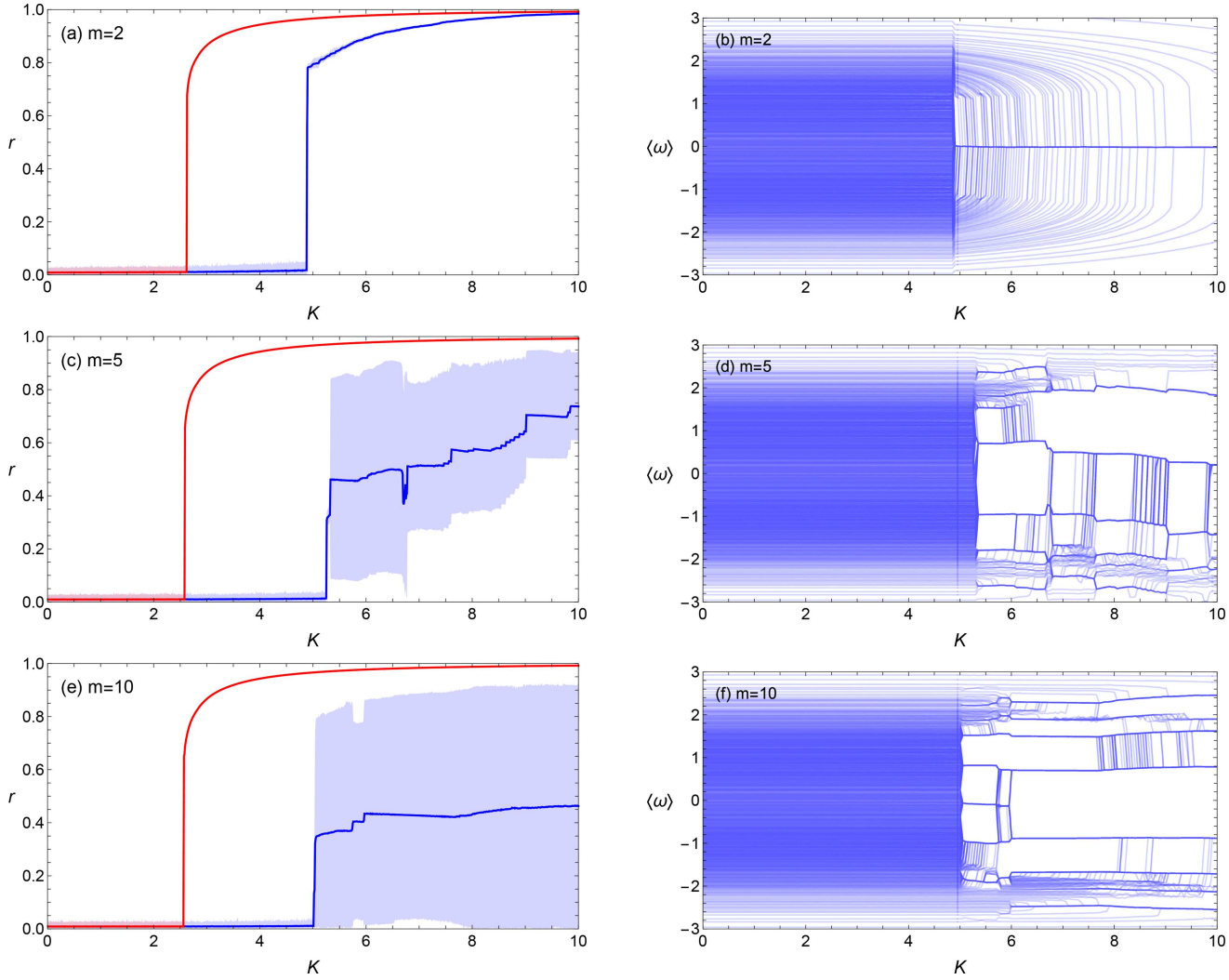

FIG. 12. Results of the numerical simulations for the forward and backward processes for $N = 10\,000$ oscillators and bimodal natural frequency distribution $g_3(\Omega)$ with strongly overlapping modes. The inertias considered in these pictures are $m = 2$ (top row), $m = 5$ (middle row), and $m = 10$ (bottom row). The description of the panels at the left and right sides is as in Fig. 1.

2. Standing waves

We now apply a similar analysis as in Sec. III A to standing wave states. We are assuming that $r e^{i\phi} = \varepsilon f(t)\, e^{i(\Omega^r t+\phi_0)}$ where, as before, $f(t)$ has zero average and is periodic with period T. In this case, the mean field equations become

$$\dot{\theta} = \omega, \tag{A4a}$$

$$m\dot{\omega} + D\omega = D\,\Delta\Omega - K\varepsilon f(t)\sin(\theta), \tag{A4b}$$

where $\Delta\Omega = (\Omega/D) - \Omega^r$.

For $\varepsilon = 0$, the system has a stable limit cycle L given by $\omega = \Delta\Omega$ and the rotation number of the corresponding Poincaré map is $\mathrm{rot}(F) = \Delta\Omega$. As ε starts increasing the limit cycle persists as an invariant curve L_ε. However, for larger values of ε, the dynamics on L_ε will give rise to fixed points when the inertia is large enough (see Fig. 14), while there may also appear stable features outside the invariant curve.

The graphs $\mathrm{rot}(F)$ vs $\Delta\Omega$ in Fig. 14 show the appearance of two plateaus at $\Delta\Omega = \pm 1$ when we take $r(t) = \varepsilon \sin t$ modeling a standing wave state. Note that the existence of these plateaus is consistent with having a standing wave state, in the sense that if we could fix the observed dynamics and populate the plateaus with oscillators drawn from a bimodal distribution $g(\Omega)$ with peaks at $\Omega = \pm 1$, then the resulting order parameter would behave as a standing wave state. This partially explains why the standing wave states appear in the case of bimodal distributions, especially when the modes are well separated.

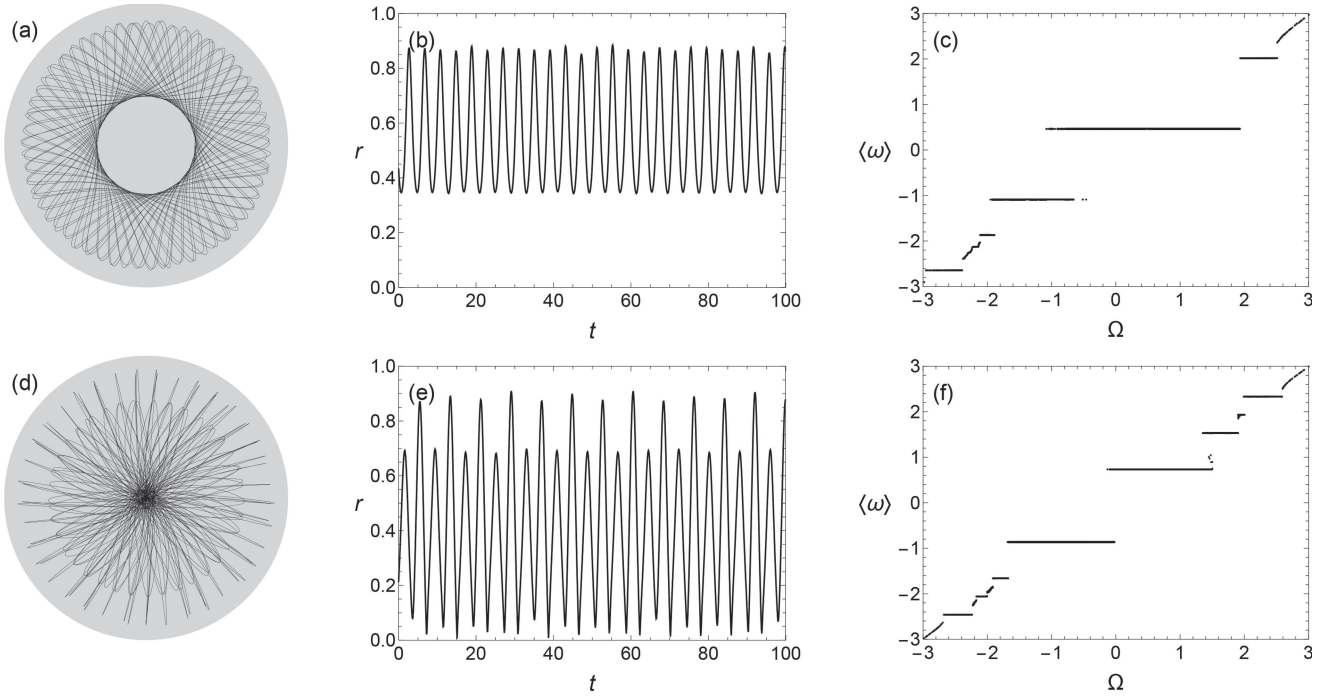

FIG. 13. States obtained from the forward process for the bimodal distribution $g_3(\Omega)$ with strongly overlapping modes. Top row: oscillatory state for $m = 5$ and $K = 8.0$; bottom row: standing wave state for $m = 10$ and $K = 8.0$. The description of the panels is as in Fig. 2.

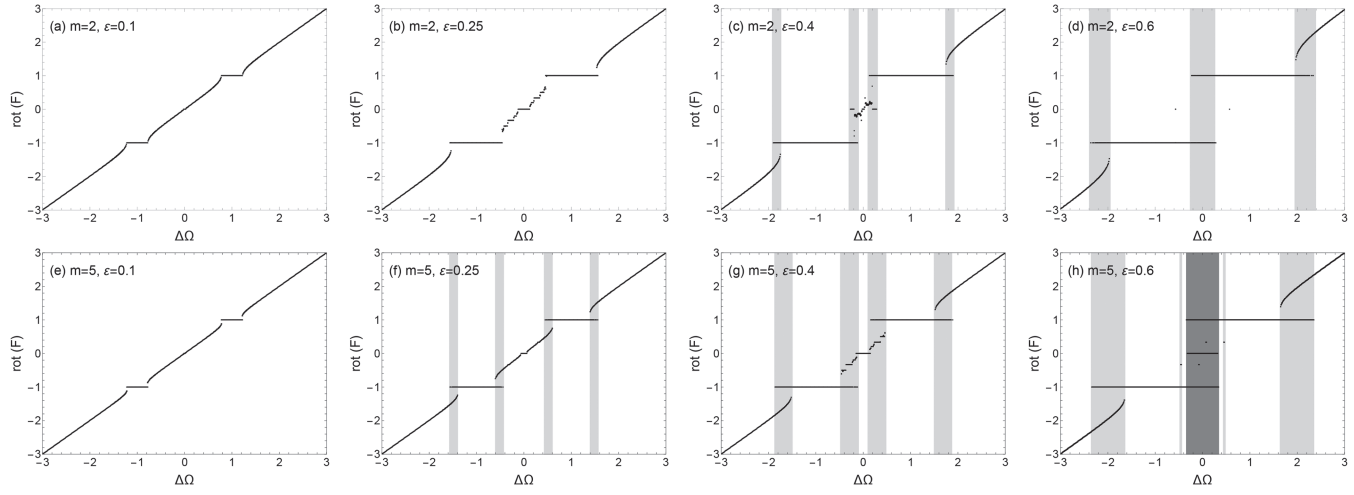

FIG. 14. Rotation number rot(F) as function of $\Delta\Omega = (\Omega/D) - \Omega^r$ for Eq. (9) with standing wave $r(t) = \varepsilon \sin t$. Top row: $m = 2$; bottom row: $m = 5$. The value of ε increases from left to right taking the values $\varepsilon = 0.1, 0.25, 0.4, 0.6$—note that for $\varepsilon = 0$, we have rot$(F) = \Delta\Omega$. In all cases, $D = 1$ and $K = 4.5$. Bistable regions are colored light gray, and multistable regions (three or more stable features) are colored dark gray. In panels (c) and (d), there are small bi- or multi-stable regions that we have not colored.

An alternative way of understanding the synchronization process and the formation of secondary synchronized clusters in the case of bimodal distributions with well separated modes is by considering the populations of oscillators around each peak of the distribution as separate systems with a weak interaction among them. Then, for small inertias, each of the populations will form a synchronized cluster and the complex order parameters for the two clusters will rotate in the opposite sense on the complex plane giving rise to the standing wave state. This can happen either in the forward or in the backward process and for small or large inertias. However, for large inertias in the forward process, each of the two populations will give rise to secondary clusters complicating the synchronization scenario. In all cases, as K increases and the interaction between the two populations becomes stronger the system will eventually reach a coherent stationary state.

DATA AVAILABILITY

The data that support the findings of this study are available from the corresponding author upon reasonable request.

REFERENCES

Acebrón, J. and Bonilla, L., "Asymptotic description of transients and synchronized states of globally coupled oscillators," Physica D **114**, 296–314 (1998).

Acebrón, J., Bonilla, L., and Spigler, R., "Synchronization in populations of globally coupled oscillators with inertial effects," Phys. Rev. E **62**, 3437 (2000).

Acebrón, J., Perales, A., and Spigler, R., "Bifurcations and global stability of synchronized stationary states in the Kuramoto model for oscillator populations," Phys. Rev. E **64**, 016218 (2001).

Acebrón, J. A., Bonilla, L. L., Vicente, C. J. P., Ritort, F., and Spigler, R., "The Kuramoto model: A simple paradigm for synchronization phenomena," Rev. Mod. Phys. **77**, 137 (2005).

Arenas, A., Díaz-Guilera, A., Kurths, J., Moreno, Y., and Zhou, C., "Synchronization in complex networks," Phys. Rep. **469**, 93–153 (2008).

Ashwin, P. and Burylko, O., "Weak chimeras in minimal networks of coupled phase oscillators," Chaos **25**, 013106 (2015).

Barre, J. and Métivier, D., "Bifurcations and singularities for coupled oscillators with inertia and frustration," Phys. Rev. Lett. **117**, 214102 (2016).

Belykh, V. N., Bolotov, M. I., and Osipov, G. V., "Kuramoto phase model with inertia: Bifurcations leading to the loss of synchrony and to the emergence of chaos," Model. Anal. Inf. Syst. **22**, 595–608 (2015).

Brister, B. N., Belykh, V. N., and Belykh, I. V., "When three is a crowd: Chaos from clusters of Kuramoto oscillators with inertia," Phys. Rev. E **101**, 062206 (2020).

Devaney, R. L., *An Introduction to Chaotic Dynamical Systems*, 2nd ed. (Westview Press, 2003).

Dörfler, F., Chertkov, M., and Bullo, F., "Synchronization in complex oscillator networks and smart grids," Proc. Natl. Acad. Sci. U.S.A. **110**, 2005–2010 (2013).

Engelbrecht, J. R. and Mirollo, R., "Structure of long-term average frequencies for Kuramoto oscillator systems," Phys. Rev. Lett. **109**, 034103 (2012).

Ermentrout, B., "An adaptive model for synchrony in the firefly *Pteroptyx malaccae*," J. Math. Biol. **29**, 571–585 (1991).

Fenichel, N., "Persistence and smoothness of invariant manifolds for flows," Indiana Univ. Math. J. **21**, 193–226 (1971).

Filatrella, G., Nielsen, A. H., and Pedersen, N. F., "Analysis of a power grid using a Kuramoto-like model," Eur. Phys. J. B **61**, 485–491 (2008).

Gambuzza, L. V., Buscarino, A., Fortuna, L., Porfiri, M., and Frasca, M., "Analysis of dynamical robustness to noise in power grids," IEEE J. Emerg. Sel. Top. Circuits Syst. **7**, 413–421 (2017).

Gao, J. and Efstathiou, K., "Self-consistent method and steady states of second-order oscillators," Phys. Rev. E **98**, 042201 (2018).

Goldschmidt, R. J., Pikovsky, A., and Politi, A., "Blinking chimeras in globally coupled rotators," Chaos **29**, 071101 (2019).

Gómez-Gardeñes, J., Gómez, S., Arenas, A., and Moreno, Y., "Explosive synchronization transitions in scale-free networks," Phys. Rev. Lett. **106**, 128701 (2011).

Grzybowski, J., Macau, E., and Yoneyama, T., "On synchronization in power-grids modelled as networks of second-order Kuramoto oscillators," Chaos **26**, 113113 (2016).

Guckenheimer, J. and Holmes, P. J., *Nonlinear Oscillations, Dynamical Systems, and Bifurcations of Vector Fields* (Springer Science & Business Media, 2013), Vol. 42.

Hellmann, F., Schultz, P., Grabow, C., Heitzig, J., and Kurths, J., "Survivability of deterministic dynamical systems," Sci. Rep. **6**, 29654 (2016).

Hirsch, M. W., Pugh, C. C., and Shub, M., "Invariant manifolds," Bull. Am. Math. Soc. **76**, 1015–1020 (1970).

Ikeda, Y., Aoyama, H., Fujiwara, Y., Iyetomi, H., Ogimoto, K., Souma, W., and Yoshikawa, H., "Coupled oscillator model of the business cycle with fluctuating goods markets," Progr. Theor. Phys. Suppl. **194**, 111–121 (2012).

Kim, H., Lee, S. H., and Holme, P., "Community consistency determines the stability transition window of power-grid nodes," New J. Phys. **17**, 113005 (2015).

Kruk, N., Maistrenko, Y., and Koeppl, H., "Solitary states in the mean-field limit," Chaos **30**, 111104 (2020).

Kuramoto, Y., "Self-entrainment of a population of coupled non-linear oscillators," in *International Symposium on Mathematical Problems in Theoretical Physics*, Lecture Notes in Physics Vol. 39, edited by H. Araki (Springer, 1975), pp. 420–422.

Kuramoto, Y., *Chemical Oscillations, Waves, and Turbulence* (Springer-Verlag, 1984).

Kuramoto, Y. and Nishikawa, I., "Statistical macrodynamics of large dynamical systems. Case of a phase transition in oscillator communities," J. Stat. Phys. **49**, 569–605 (1987).

Levi, M., Hoppensteadt, F. C., and Miranker, W. L., "Dynamics of the Josephson junction," Q. Appl. Math. **36**, 167–198 (1978).

Lozano, S., Buzna, L., and Díaz-Guilera, A., "Role of network topology in the synchronization of power systems," Eur. Phys. J. B **85**, 1–8 (2012).

Maïzi, N., Krakowski, V., Assoumou, E., Mazauric, V., and Li, X., "Time reconciliation and space aggregation to shed light on the plausibility of long-term low carbon pathways for power systems," in *Smart Energy Grid Engineering (SEGE), 2016 IEEE* (IEEE, 2016), pp. 106–110.

Manik, D., Rohden, M., Ronellenfitsch, H., Zhang, X., Hallerberg, S., Witthaut, D., and Timme, M., "Network susceptibilities: Theory and applications," Phys. Rev. E **95**, 012319 (2017).

Medvedev, G. S. and Mizuhara, M. S., "Stability of clusters in the second-order Kuramoto model on random graphs," J. Stat. Phys. **182**, 21 (2021).

Menck, P. J., Heitzig, J., Marwan, N., and Kurths, J., "How basin stability complements the linear-stability paradigm," Nat. Phys. **9**, 89–92 (2013).

Métivier, D., Wetzel, L., and Gupta, S., "Onset of synchronization in networks of second-order Kuramoto oscillators with delayed coupling: Exact results and application to phase-locked loops," Phys. Rev. Res. **2**, 023183 (2020).

Munyaev, V. O., Smirnov, L. A., Kostin, V. A., Osipov, G. V., and Pikovsky, A., "Analytical approach to synchronous states of globally coupled noisy rotators," New J. Phys. **22**, 023036 (2020).

Olmi, S., Navas, A., Boccaletti, S., and Torcini, A., "Hysteretic transitions in the Kuramoto model with inertia," Phys. Rev. E **90**, 042905 (2014).

Olmi, S. and Torcini, A., "Dynamics of fully coupled rotators with unimodal and bimodal frequency distribution," in *Control of Self-Organizing Nonlinear Systems* (Springer, 2016), pp. 25–45.

Pinto, R. S. and Saa, A., "Synchrony-optimized networks of Kuramoto oscillators with inertia," Physica A **463**, 77–87 (2016).

Rodrigues, F. A., Peron, T. K. D., Ji, P., and Kurths, J., "The Kuramoto model in complex networks," Phys. Rep. **610**, 1–98 (2016).

Rohden, M., Sorge, A., Timme, M., and Witthaut, D., "Self-organized synchronization in decentralized power grids," Phys. Rev. Lett. **109**, 064101 (2012).

Rohden, M., Sorge, A., Witthaut, D., and Timme, M., "Impact of network topology on synchrony of oscillatory power grids," Chaos **24**, 013123 (2014).
Rohden, M., Witthaut, D., Timme, M., and Meyer-Ortmanns, H., "Curing critical links in oscillator networks as power flow models," New J. Phys. **19**, 013002 (2017).
Sakyte, E. and Ragulskis, M., "Self-calming of a random network of dendritic neurons," Neurocomputing **74**, 3912–3920 (2011).
Strogatz, S. H., *Nonlinear Dynamics and Chaos: With Applications to Physics, Biology, Chemistry, and Engineering* (Westview Press, 2014).
Tanaka, H.-A., Lichtenberg, A. J., and Oishi, S., "First order phase transition resulting from finite inertia in coupled oscillator systems," Phys. Rev. Lett. **78**, 2104 (1997).
Tanaka, H.-A., Lichtenberg, A. J., and Oishi, S., "Self-synchronization of coupled oscillators with hysteretic responses," Physica D **100**, 279–300 (1997).
Trees, B., Saranathan, V., and Stroud, D., "Synchronization in disordered Josephson junction arrays: Small-world connections and the Kuramoto model," Phys. Rev. E **71**, 016215 (2005).
Tumash, L., Olmi, S., and Schöll, E., "Effect of disorder and noise in shaping the dynamics of power grids," Europhys. Lett. **123**, 20001 (2018).
Tumash, L., Olmi, S., and Schöll, E., "Stability and control of power grids with diluted network topology," Chaos **29**, 123105 (2019).
Watanabe, S. and Strogatz, S. H., "Constants of motion for superconducting Josephson arrays," Physica D **74**, 197–253 (1994).
Witthaut, D., Rohden, M., Zhang, X., Hallerberg, S., and Timme, M., "Critical links and nonlocal rerouting in complex supply networks," Phys. Rev. Lett. **116**, 138701 (2016).
Witthaut, D. and Timme, M., "Braess's paradox in oscillator networks, desynchronization and power outage," New J. Phys. **14**, 083036 (2012).